Research Paper

Plumbagin has an inhibitory effect on the growth of TSCC PDX model and it enhances the anticancer efficacy of cisplatin

Yuqi Xin[1,2], Qingkun Jiang[1,2], Chenshu Liu[1,2], Jiaxuan Qiu[1]

[1]Department of Stomatology, The First Affiliated Hospital of Nanchang University, Nanchang, Jiangxi 330006, China
[2]Medical College, Nanchang University, Nanchang, Jiangxi 330006, China

Correspondence to: Jiaxuan Qiu; **email:** qiujiaxuan@163.com, https://orcid.org/0000-0002-3335-0782
Keywords: tongue squamous cell carcinoma (TSCC), patient-derived xenograft (PDX), plumbagin, proliferation, prognosis
Received: June 6, 2023 **Accepted:** October 2, 2023 **Published:** November 3, 2023

ABSTRACT

Background: Head and neck squamous cell carcinomas are the sixth most common malignant tumors worldwide. Tongue squamous cell carcinoma is a common malignant tumor of this type, and it is associated with poor prognosis, a high rate of recurrence and a low survival rate. Plumbagin is derived from Plumbago zeylanica L, several studies report that plumbagin could inhibit cell, tumor metastasis, induce apoptosis in various cancer cells. Patient-derived xenograft (PDX) model can maintain the heterogeneity and microenvironment of human tumors, is a powerful research tool for developing potentially effective therapies for TSCC.

Methods: Tumor tissues obtained from TSCC patients were implanted into immunodeficient mice to establish TSCC PDX models. Subsequently, the PDX models were used to evaluate the anti-tumor effects of plumbagin on TSCC. Furthermore, we conducted next-generation sequencing (NGS) and explored the mRNA expression profiles between the treatment and control groups. We selected eight mRNAs related to the characteristics and prognosis of TSCC patients for further analysis.

Results: Plumbagin could inhibit the growth of TSCC PDX models and inhibit expression of Akt/mTOR pathway. In addition, plumbagin was shown to increase drug sensitivity to cisplatin. The eight mRNAs selected for further analysis, AXL, SCG5, VOPP1, DCBLD2 and DRAM1 are cancer-promoting genes, DUSP1, AQP5 and BLNK are cancer suppressor genes. And they were related to the diagnosis, growth, prognosis, and immune cell infiltration in TSCC patients.

Conclusion: Plumbagin exhibits an inhibitory effect on the growth of the PDX model of TSCC. Moreover, plumbagin enhances the inhibitory effects of cisplatin.

INTRODUCTION

Head and neck squamous cell carcinoma (HNSCC) are the sixth most common malignant tumors worldwide. [1]. Tongue squamous cell carcinoma (TSCC) accounts for 25–40% of oral cancers. It is one of the most aggressive types of HNSCC [2–4], associated with poor prognosis, a high risk of relapse, and a 5-year survival rate of less than 50% [5–8]. According to previous studies, about 40–60% of patients show local recurrence or lymph node metastasis within five years of treatment [9, 10]. Therefore, complete recovery is not achieved despite the widespread use of advanced diagnostic techniques and therapies, such as surgery, chemotherapy, and radiotherapy [11–13]. Thus, there is an urgent need for researchers to understand the genetic and molecular mechanisms behind the carcinogenesis, and develop clinically relevant biomarkers and new treatment

methods. However, little progress has been made in developing effective therapies as there are no models that mimick the biological characteristics of TSCC. Therefore, researchers need to develop a high-fidelity model that can reflect the biological characteristics of TSCC.

Intratumoral heterogeneity and microenvironment are critical in cancer progression, evolution, and response to therapy [14, 15]. Patient-derived xenograft (PDX) models are transplanted tumor models formed by implanting tissue blocks, circulating tumor cells, and primary cells from tumor patients into immunodeficient mice [16, 17]. The PDX models can maintain the heterogeneity and microenvironment of tumors, thus mimic human cancers and effectively predict response to therapy [16, 17]. Moreover, drug sensitivity testing using the PDX model has approximately 90% clinical relevance [18], indicating that the PDX model is a powerful tool for personalized and precise cancer treatment.

Phytochemicals are naturally occurring compounds of plant origin, in recent years, many studies have proved that they can directly or indirectly target multiple signal pathways of cancer cells and have been widely used to treat a variety of cancers [19]. At present, there is evidence that the combination of many phyto-chemicals and traditional anticancer drugs can play a significant role in improving the efficacy of single therapy, resisting drug resistance, and reducing organ toxicity [20, 21]. Plumbagin (5-hydroxy-2-methyl-1,4-naphthoquinone) is a traditional Chinese medicine (TCM) and is a small molecular weight compound derived from the roots of Plumbago zeylanica L [22]. Recent evidence shows that plumbagin could inhibit cell proliferation, tumor metastasis by inducing apoptosis of various cancer cells [23, 24]. Further, previous studies show that plumbagin could inhibit cell growth, migration, and invasion by inducing apoptosis of tongue squamous cell carcinoma cells in humans [25–27].

This study aimed to evaluate the anti-tumor effects of plumbagin on TSCC using next-generation sequencing and other techniques. Therefore, we established 14 PDX models of human tongue squamous cell carcinoma, which were then treated with plumbagin.

MATERIALS AND METHODS

Patient and tissue samples

Tumor samples were collected from 18 patients with TSCC during surgical procedures between December 2017 to April 2019, and processed tumor tissue within 24 hours. The criteria for selecting patients are that pathological findings confirmed squamous cell carcinoma, the tumor is located in the tongue, no distant metastasis, and they have not been treated before. Written informed consent was obtained from the patients and the patients agreed to use their tissues in the research. We have successfully established 14 TSCC PDX models. (Table 1). These were provided by the Department of Oral and Maxillofacial Surgery, the First Affiliated Hospital of Nanchang University. The study was conducted with prior approval of The First Affiliated Hospital of Nanchang University Ethics Committee (Permit No. (2022) CDYFYYLK (11-002)).

Materials

The plumbagin (Lot. No. 1012D021) was purchased from Solarbio Science and Technology Co., Ltd., (Beijing, China). The cisplatin (H20040813) was purchased from Haosen Pharmaceutical Co., Ltd., (Jiangsu, China). The hematoxylin staining solution (ZLI-9610) was purchased from Zhongshan Jinqiao Biotechnology Co., Ltd., (Beijing, China). The Scott blue solution (G1865) and the eosin dye solution (G1100) were purchased from Solarbio Science and Technology Co., Ltd., (Beijing, China). 30 mg plumbagin was dissolved in 1 mL DMSO and added 39 mL 0.9% saline, protected from light, stored at −20°C.

Balb/c nude mice aged 6 weeks (Hangzhou Ziyuan Laboratory Animal Technology Co., Ltd., Zhejiang, China, License number: SCXK2019-0004) were used for PDX establishment and treatment research. They were reared in an SPF environment.

Establishment of patient-derived xenografts (PDX) for TSCC

The fresh surgically resected TSCC tissues were cut into 2 mm × 2 mm × 2 mm (8 mm^3) sections within 24 hours, and evident necrosis, liquefaction tissues were removed. Sections were inoculated subcutaneously into the scapular region of 8-weeks-old female BALB/c nude mice and were numbered as P0. When the tumor volume grew to more than 1,000 mm^3, the tumor was resected and cut into 2 mm × 2 mm × 2 mm (8 mm^3) sections, subcutaneously were inoculated into the scapular region of BALB/c nude mice, numbered P1, and the tumors were passaged to P4 by the same method and used for subsequent experimental research. The implantation procedure was carried out as previously described [28].

Table 1. Characteristics of the patients.

	n = 14
Age (years):	
≤65	8
>65	6
Sex:	
Male	11
Female	3
Tumor size (cm):	
≤2	0
>2, ≤4	2
>4	12
Differentiation:	
Well	3
Moderate/low	11
Cervical lymph node metastasis:	
Yes	7
No	7
Clinical Staging:	
II	1
III	7
IV	6

Anti-cancer treatment

When the average tumor volume reached 100–200 mm^3, the mice were randomized into different treatment cohorts (n = 5): control group (0.9% saline, 0.1 ml once a day, intraperitoneal injection), cisplatin group (5 mg/kg once a week, intraperitoneal injection) [29], plumbagin group (2 mg/kg once a day, intraperitoneal injection) [30], and plumbagin + cisplatin group (the drug dosage and administration were the same as before). The tumor volume and the bodyweight were recorded every three days. The animals were sacrificed after 21 days (mice were injected intraperitoneally with sodium pentobarbital 150 mg/kg and mice were anesthetized and then euthanized by cervical dislocation), when the tumor volume in the control group reached 1,000 mm^3. The tumors were then excised, weighed, and cut into two halves. One-half of the tumor samples were fixed in formalin, while the other half was stored in liquid nitrogen. Moreover, the hearts, livers, spleens, lungs, and kidneys were fixed in formalin. Tumor volume was calculated using the formula: length × $width^2$ × 0.5, the measuring tool is a vernier caliper.

Hematoxylin-eosin (HE) staining

The tissue samples were rinsed with water, dehydrated using ethanol solutions (70%, 80%, and 90%), embedded in paraffin, and finally sectioned. The paraffin sections were baked in an oven, dewaxed, hydrated, and then placed in an aqueous solution of hematoxylin for 3 min. After that, hydrochloric acid ethanol solution was applied for 15 s for differentiation, followed by washing with water. Moreover, the sections were placed in Scott solution for 15 s for blueing, rinsed with water, stained with eosin for 3 min, rinsed with running water, dehydrated, and sealed.

Immunohistochemistry (IHC) staining

The tissue slices were immersed in 0.01 M citrate buffer (pH 6.0, Wellbio, Shanghai, China). The buffer was heated to boiling and cooked for 20 minutes, then cooled to room temperature. After cooling, the tissue slices were washed with PBS (pH 7.2~7.6, Wellbio, Shanghai, China). The diluted primary antibody (Ki67, Abcam, Cambridge, United Kingdom) was then added to the tissue samples and incubated at 4°C overnight. After that, the tissue slices were washed with PBS and were added 50~100 ul of anti-rabbit-IgG antibody-HRP polymer (Thermo Fisher Scientific, Shanghai, China). Further, 50~100 ul of a working solution of chromogenic reagent DAB (diaminobenzidine, Zhongshan Jinqiao Biotechnology Co., Ltd., Beijing, China) was added. The tissues were counter-stained with hematoxylin and mounted with neutral gum (Sigma, USA). Nuclear Ki-67 stained brown. The Ki67 slides were analyzed using a

microscope (Olympus, Tokyo, Japan, BX43). Six 400X images were analyzed for each slide. The positivity cell rate was calculated as the ratio of the number of positive cells to the number of total cells.

Short tandem repeat (STR) analysis

STRs are mainly used in genetic linkage map analysis, family identification, identity authentication, and other fields. We used the TIANamp genomic DNA kit to extract an appropriate amount of DNA from patient tumor tissue and PDX model tumor tissue, 20 STR loci and gender identification loci were amplified by MicroreaderTM21 ID System, PCR product detection was performed by GenReader 7010 genetic analyzer, detection results were analyzed by GeneMapper Software 6 (Applied Biosystems, USA) and compared with ExPASy databases.

Next-generation sequencing

Genomic data were extracted from the PDX models for tongue squamous cell carcinoma (n = 3 in each group, from PDX models No. 3, 6, and 12) obtained from the four treatment groups and were mass-cut using Trimmomatic software version 0.36. Further, the data were compared to the reference genome using HISAT2 software version 2.1.0. For statistics mapping information, in addition, RSeQC software version 2.6.1, Qualimap software version 2.2.1, BEDTools software version 2.26.0 were used for analysis based on the results. After that, ASprofier software version 1.0.4 and EricScript software version 0.55 were used for genetic analysis. Moreover, StringTie software version 1.3.3b and R package WGCNA version 1.51 were used to analyze gene expression. Finally, differences in gene expression were analyzed using the R package DESeq version 1.26.0. The threshold for significant differential expression was set at p value < 0.05 and fold-change >2 or fold-change <0.5.

Reverse transcription-quantitative polymerase chain reaction (RT-qPCR)

Tumor tissue was lysed by Trizol reagent (Kangwei Century, CW0580S, CWBIO, China), chloroform and isopropanol were added, then 75% ethanol was added after centrifugation. After the total RNA was extracted, a reverse transcription kit (Guangzhou Ribo Biological Co., Ltd., Guangzhou, China) was used to synthesize cDNA. The mixture was prepared according to the instructions of Takara TB Green Premix Ex TaqIIRT-PCR Kit. The RT-qPCR analysis was performed on Step One Plus Real-Time PCR System. Each experiment was repeated 3 times. The $2^{-\Delta\Delta CT}$ method was used to calculate the expression level of the related RNAs. Moreover, the related GAPDH mRNA expression was used as an endogenous control. The primers used are shown in Table 2.

Western blot (WB) analysis

The tissue protein of the PDX model was extracted with cell lysis buffer (Beyotime, Shanghai, China). Protein content was determined using a BCA Protein Assay Kit (Bio-Rad, USA). Then, the protein sample was heated to 100°C and incubated for 5 minutes, electrophoresis was performed on SDS-PAM gel and transferred to the polyvinylidene fluoride (PVDF) membrane. The membrane was sealed with 5% skimmed milk for 80 min and incubated with the primary antibody (anti-rabbit monoclonal antibody AKT, p-AKT, mTOR, p-mTOR, 1:1,000, CST, USA; anti-rabbit monoclonal antibody β-actin, AXL, SCG5, VOPP1, DCBLD2, DRAM1, DUSP1, AQP5 and BLNK 1:2,000, Proteintech, China) at 4°C overnight. The membrane was incubated with the goat anti-rabbit secondary antibody (1:5,000, Proteintech, China) for 1 h the next day. And membrane was soaked with luminescent liquid, placed in an ultra-high sensitivity chemiluminescence imaging system (Chemi DocTM XRS+, Bole Life Medical Products Co., Ltd., Shanghai, China) for image generation. Finally, images were analysed with ImageJ software.

Receiver operating characteristic (ROC) curves

The performance discrimination and diagnostic accuracy for mRNA were evaluated by constructing ROC curves and estimating the area under the curve (AUC) of patient with oral squamous cell carcinoma (OSCC) versus controls. Clinical data of OSCC patients were obtained from the TCGA Database (https://portal.gdc.cancer.gov/). Analysis was performed using the pROC package (version 1.17.0.1) in R (version 4.1.2).

Immune infiltration analysis using ssGSEA

The immune signature score was calculated using the single-sample gene set enrichment analysis (ssGSEA2.0) implemented by the GSVA package (version 1.34.0) in R (version 4.1.2). Based on the characteristic genes of 24 different immune cell types, the relative immune cell tumor infiltration level was quantified from the gene expression profiles of each tumor sample. Spearman correlation analysis was used to analyze the correlation between AXL, SCG5, VOPP1, DCBLD2, DRAM1, DUSP1, AQP5, BLNK

Table 2. Sequence of primers.

Primer name	Primer sequence
DRAM1 F	TGTCGCCAATTTTCAGGAGTT
DRAM1 R	TCCGTATGTGGCATGTCGAG
BLNK F	AAGTCAAAGGCCCTCCAAGT
BLNK R	CGGAGTCCGAATGTTCATCT
AQP5 F	GCCCTCTTAATAGGCAACCAG
AQP5 R	GCATTGACGGCCAGGTTAC
DUSP1 F	GCCACCATCTGCCTTGCTTACC
DUSP1 R	ATGATGCTTCGCCTCTGCTTAC
DCBLD2 F	ATGTGGACACACTGTACTAGGC
DCBLD2 R	CTGTTGGGATAGGTCTGTGG
VOPP1 F	GATGAACCCTGTCGGGAAT
VOPP1 R	GGCCTTCACTACCTGTTCGTA
SCG5 F	GGGTCCTTTTGGCAACATCC
SCG5 R	CCCCTGATCCTCACTAAAGTCC
AXL F	GACCGGCCAAGTTTTACAGA
AXL R	ATAACCTCCACCCTCATCCA
GAPDH F	TGACTTCAACAGCGACACCCA
GAPDH R	CACCCTGTTGCTGTAGCCAAA

and the level of immune cell infiltration. Further, the Wilcoxon rank-sum test was used to analyze the correlation between immune cell infiltration and the expression of different mRNAs.

Statistical analysis

All calculations were performed by SPSS 22.0 (IBM Corp., USA) and GraphPad Prism software version 7.0 (GraphPad Software, Inc., USA). Differences between groups were analyzed by using one-way ANOVA following the post-hoc tests by Tukey. Data were presented as mean ± standard deviation (SD). $P < 0.05$ was considered statistically significant.

Availability of data and materials

The datasets used and/or analyzed during the current study are available from the corresponding author on reasonable request.

RESULTS

Establishment of patient-derived xenografts

Eighteen TSCC samples were implanted under the skin of immunodeficient mice, to obtain the P0 generation. Subsequently, 14 PDX models of TSCC were successfully established. The tumor formation rate in the TSCC PDX models was about 77.8%, with an average tumor formation period of 86.4 days. The implanted tumors were passaged to four times to generate four generations (P1, P2, P3, and P4). The P4 generation model was used for subsequent experiments. The tumor formation rate increased as the passaging of the generations was increased. However, the tumor formation time decreased as the generations increased. On the other hand, the formation time of the models gradually stabilized after the P1 generation (Table 3, Figure 1).

Histological analysis and STR analysis of the xenograft tumors

A total of 14 TSCC PDX models were established. An examination of the patient-derived xenografts and the original tumor samples showed that the proliferating epithelium of the PDX models invaded the connective tissue. In addition, the nucleus showed deep staining. However, the cytoplasm was less stained, and the cell boundary was unclear. There was a similar growth pattern and morphology between the PDX xenografts and the original tumor samples (Figure 2).

The DNA samples of patients and PDXs were tested for STR genotyping. The STR data showed no cross

Table 3. Tumor formation rate and time of TSCC PDX model.

	Tumor formation rate (%)	Tumor formation time (d)
P0	77.8	86.4 ± 70.9
P1	78.6	35.7 ± 10.3
P2	81.8	26.4 ± 4.9
P3	88.9	21.0 ± 1.9
P4	100	20.0 ± 1.1

contamination of human cells was found in these tumor samples. STR analysis results showed that the two STR data conformed to the law of inheritance, had the same locus information and can be judged as the same individual source (Supplementary Figure 1).

The anti-tumor effect of plumbagin on tongue squamous cell carcinoma

The anti-tumor activity of plumbagin was evaluated in the TSCC PDX models. Plumbagin was administered via intraperitoneal injection at a dose of 2 mg/kg daily, and cisplatin was administered via intraperitoneal injection at a dose of 5 mg/kg once a week. Treatment with plumbagin for 21 days showed an inhibitory effect on TSCC tumor growth. Moreover, the combination group showed the greatest inhibitory effect on tumor growth (Figure 3A–3D). These results suggested that plumbagin shows anti-tumor effects on PDX models of TSCC. Furthermore, plumbagin could enhance the anti-tumor effects of cisplatin.

Analyzing the body weight of the mice of the PDX model, it was found that there was no statistical difference in the body weight changes of the mice in each group (Figure 3E). The H&E stained sections of the heart, liver, spleen, lung, and kidney of the mice were observed. The results showed that the H&E staining of the heart, liver, spleen, lung and kidney of each group of mice did not show any organ-related toxicity (Figure 4).

The anti-proliferation effect of plumbagin

The immunohistochemistry results showed a reduced rate of Ki67 positive cells in the treatment groups compared to the control group. Furthermore, the cisplatin plus plumbagin group showed the lowest detection rate of Ki67 positive cells (Figure 5). These results suggested that plumbagin could effectively inhibit the proliferation of tumor cells in TSCC PDX models. Moreover, plumbagin could enhance the anti-proliferative effects of cisplatin.

Plumbagin affected Akt/mTOR expression in TSCC PDX models

Our previous study demonstrated that plumbagin induced apoptosis in TSCC cells, and inhibited the AKT/mTOR signaling pathway. Further, plumbagin showed synergistic effects with cisplatin in inhibiting the growth of TSCC cells [23]. We examined the effect of plumbagin on Akt/mTOR activation in TSCC PDX models. In the presence of cisplatin or plumbagin, phosphorylated Akt/mTOR was downregulated.

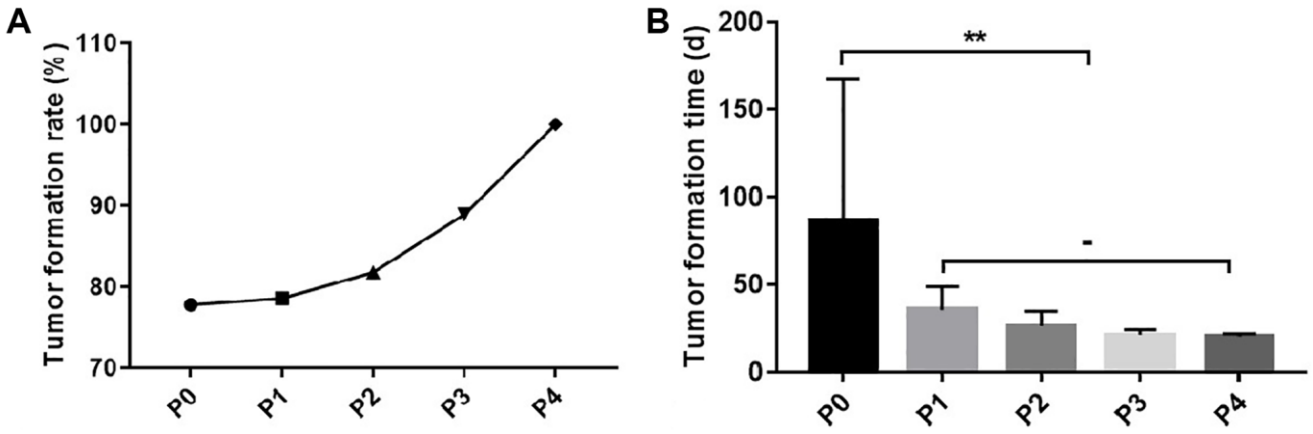

Figure 1. Tumor formation rate and time of TSCC PDX model. (**A**) The tumor formation rate of the P1-P4 generation PDX models. (**B**) The tumor formation time of the P1-P4 generation PDX models. $^{**}p < 0.01$; –, no statistical difference.

Moreover, the combination group showed phosphorylated Akt/mTOR was most significantly downregulated (Figure 6). These results suggested that plumbagin could inhibit the Akt/mTOR pathway. Moreover, plumbagin showed synergistic effects with cisplatin in inhibiting the growth of TSCC PDX models.

The expression profile of messenger RNAs (mRNAs) in TSCC PDX models

Next-generation sequencing and bioinformatics approaches were used to analyze and compare the mRNA expression profiles of tumor tissues in the four groups to determine the genes affected by plumbagin. Scatter and volcano plots were used to show the changes in mRNA expression in the four groups (Figure 7). A total of 124 upregulated mRNAs and 59 downregulated mRNAs were identified in the plumbagin group compared with the control group. Moreover, 383 upregulated mRNAs and 364 downregulated mRNAs were identified in the cisplatin group compared with the control group. In addition, 17 upregulated mRNAs and 23 downregulated mRNAs were identified in the cisplatin plus plumbagin group

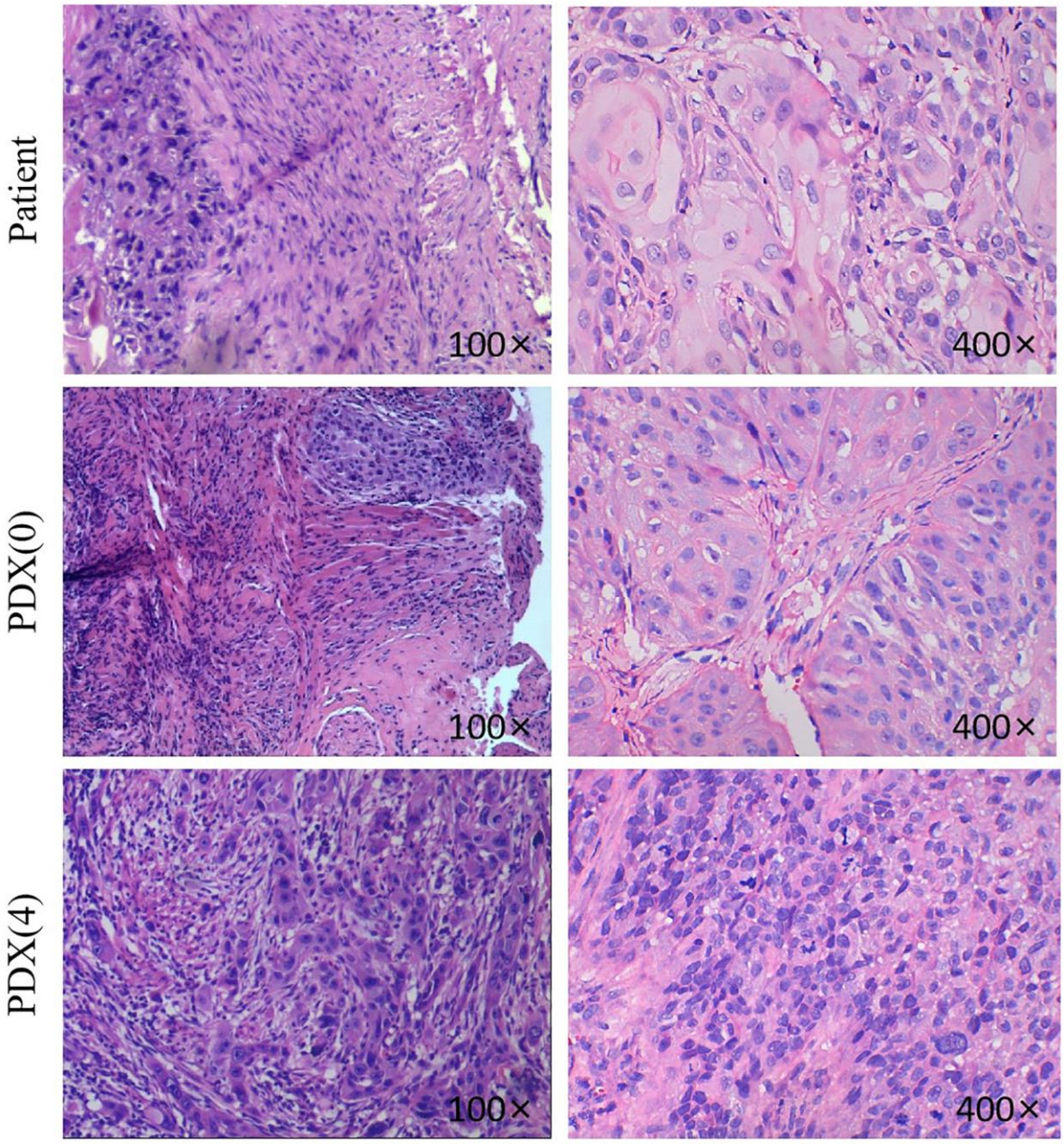

Figure 2. H&E pictures of the TSCC patients and PDX models. Histological analysis of tumor samples. After sacrificing the mice, TSCC tissues from patient and PDX models were fixed and checked with hematoxylin/eosin-staining. Cell nuclei were stained with hematoxylin (purple). The 400x and the 100x were not from the same section.

compared with the control group (Supplementary Tables 1–3). Moreover, hierarchical clustering analysis showed the differentially expressed mRNAs. The top 10 upregulated mRNAs and top 10 downregulated mRNAs were then listed (Figure 8). Further, five mRNAs were randomly selected to validate the results of RNA sequencing and evaluate their relative expression (Supplementary Figure 2). The RT-qPCR revealed that the results of RNA-seq were reliable and showed the abnormally expressed mRNAs in TSCC.

Further, we selected eight candidates with significant *p*-values ($P < 0.001$) from four groups of the abnormally expressed mRNAs to determine the mRNAs that promote or inhibit tumor growth in tongue squamous cell carcinoma. The results revealed five cancer-promoting genes (AXL, SCG5, VOPP1, DCBLD2, DRAM1), and three tumor suppressor genes (DUSP1, AQP5, BLNK). Further, based on OSCC project (RNAseq data in level 3 HTSeq-FPKM format, discard data without clinical information, and retain samples belonging to oral cancer sites in clinical information, exclude samples from non-oral cancer sites) of TCGA genome database (https://www.cancer.gov/about-nci/organization/ccg/research/structural-genomics/tcga), analysis was performed using the

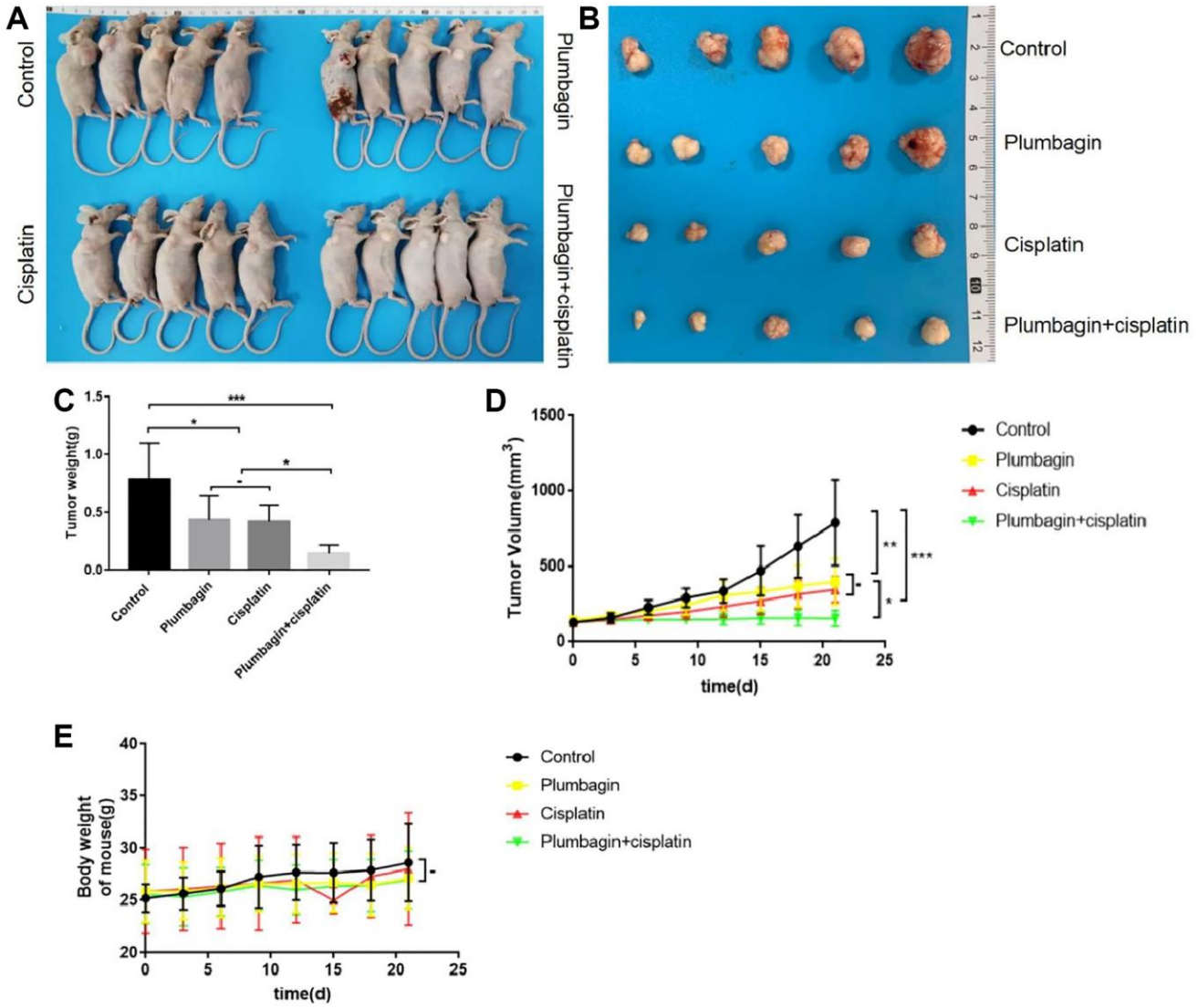

Figure 3. The anti-tumor effect of plumbagin on tongue squamous cell carcinoma. (**A**) TSCC PDX models were established. The mice were treated with plumbagin, cisplatin and their combination as described in Methods. (**B**) The tumor volume and the bodyweight were recorded every three days. The animals were sacrificed after 21 days of drug treatment. Representative samples of the PDX models showing the difference in tumor sizes between control, plumbagin, cisplatin and their combination. (**C**) Tumor weights of the PDX models were measured at the end of the experiment. (**D**) Tumor volumes of the PDX models after administration of plumbagin, cisplatin and their combination. (**E**) Body weights of the mice after administration of plumbagin, cisplatin and their combination. $^{***}p < 0.001$; $^{**}p < 0.01$; $^{*}p < 0.05$ and –, no statistical difference.

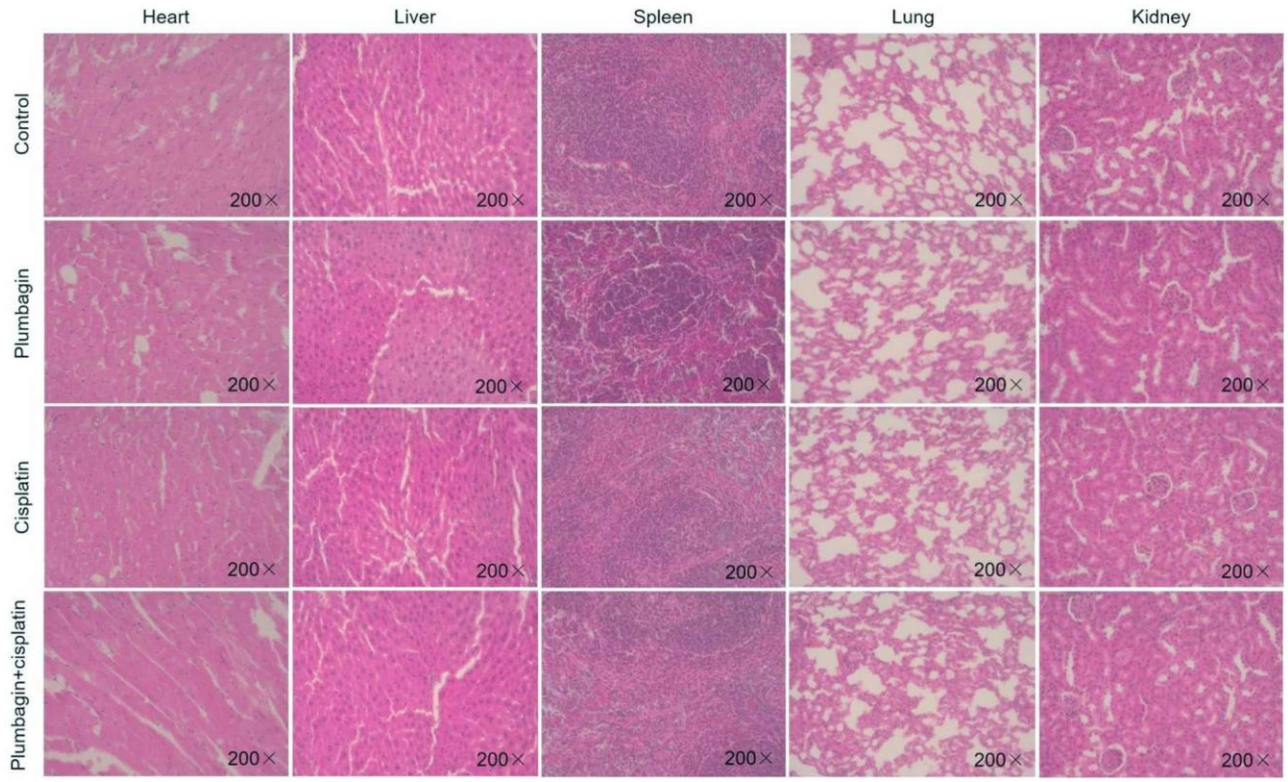

Figure 4. The hearts, livers, spleens, lungs and kidneys of mice in each model group were sliced and stained with H&E. Magnification × 200.

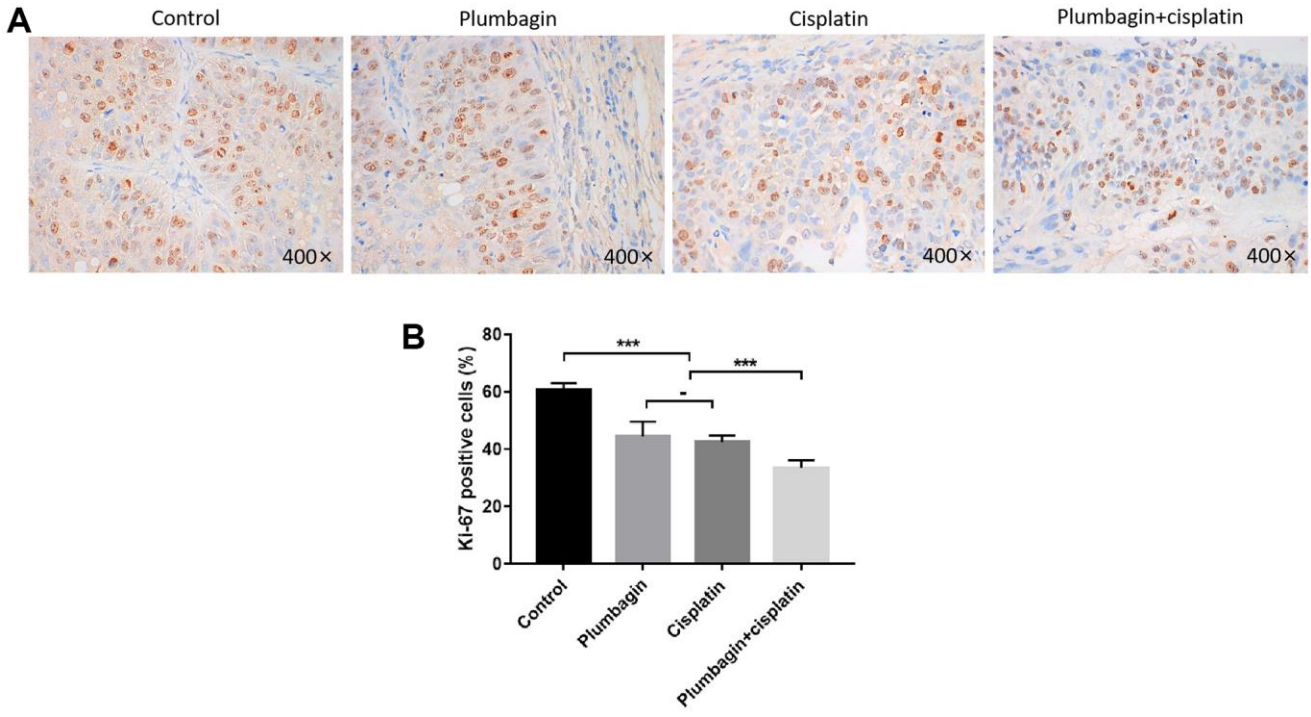

Figure 5. Anti-proliferative effect of plumbagin on TSCC PDX model. Ki67 IHC analysis was performed on each group of PDX models. (**A**) Use IHC to detect Ki67 expression. Nuclei of tumor cells were stained with hematoxylin (purple) and Ki67 positive cells have brown nuclei. (**B**) Quantitative analysis of Ki67 positive cells. Six 400X images were analyzed for each bar. Each bar represented the positivity cell rate, and the positivity cell rate was calculated as the ratio of the number of positive cells to the number of total cells. $^{***}P < 0.001$; –, no statistical difference.

ggplot2 package (version 3.3.3) and survminer package (version 0.4.9) in R (version 4.1.2), the genes were related to the prognosis in patients with oral squamous cell carcinoma (Figures 9, 10). And we used RT-qPCR to evaluate their relative expression in each treatment. The RT-qPCR results revealed that cisplatin was shown not to inhibit the expression of cancer-promoting genes. However, treatment with both plumbagin and cisplatin proved that plumbagin could potentiate the inhibitory effect of cisplatin on cancer-promoting genes. And cisplatin did not promote the expression of the tumor suppressor genes. However, treatment with both plumbagin and cisplatin has shown that plumbagin could enhance the promoting effect of cisplatin on tumor suppressor genes (Figure 11A). And we used WB to detect differential gene expression at the protein level, the WB analysis results revealed that the differentially expressed genes at the protein level were consistent with those of RT-qPCR (Figure 11B).

The receiver operating characteristic (ROC) curve for 8 biomarkers

The performance discrimination and diagnostic accuracy for mRNA were evaluated by ROC curves and AUC of patient with OSCC versus controls. The receiver operating characteristic (ROC) curve for

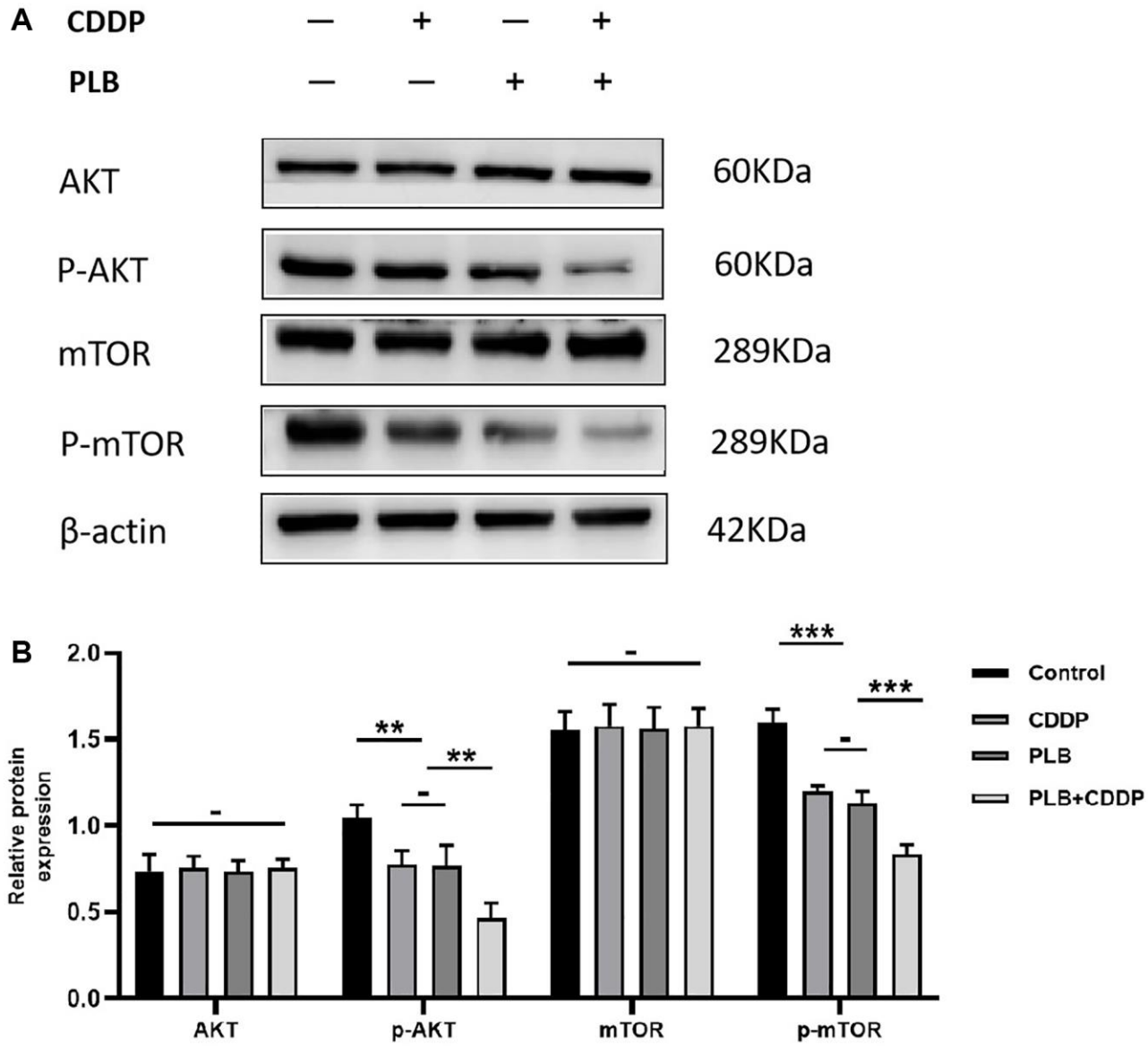

Figure 6. Administration of plumbagin affected Akt/mTOR expression in TSCC PDX models. (**A**) The expression level of AKT, p-AKT, mTOR and p-mTOR were measured by Western blotting. (**B**) The histograms indicate the relative expression levels of p-AKT/AKT, p-mTOR/mTOR. The quantitative data are shown as the mean ± SD of 3 independent experiments. ***$P < 0.001$, **$P < 0.01$ and −, no statistical difference.

8 mRNAs are shown in Figure 12. The ROC area for AXL was 0.764, the ROC area for SCG5 was 0.907, the ROC area for DCBLD2 was 0.858, the ROC area for VOPP1 was 0.860, the ROC area for DRAM1 was 0.767, the ROC area for DUSP1 was 0.725, the ROC area for AQP5 was 0.725, the ROC area for BLNK was 0.708. The area values under the ROC curve of the 8 mRNAs are all between 0.5 and 1, and the AUC are all greater than 0.65, indicating that the accuracy of diagnosis using these genes is very high.

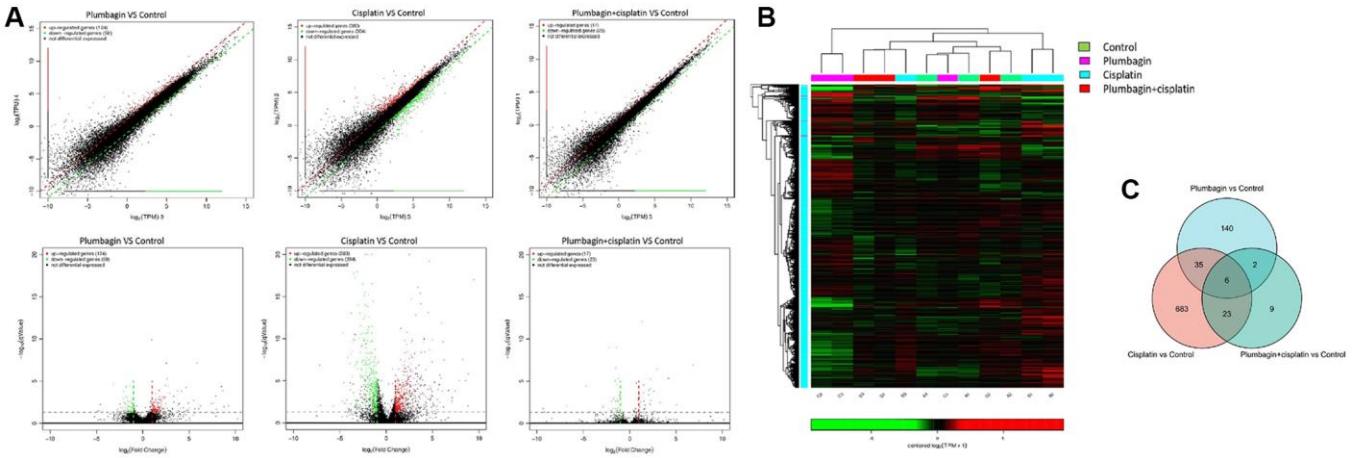

Figure 7. The mRNA expression profile among the four groups of PDX models. (**A**) Scatter plots and volcano plots showing the changes in mRNA expression between tumor tissues in the treatment groups and the control group. The horizontal and vertical axes on the scatter diagram are the two sets of sample log 2 (TPM) values. Each point in the figure represents a gene, and the closer the point is to the origin, the lower the expression level. Red represents the upregulated genes, green represents the downregulated genes, and black represents non-differentially expressed genes. The horizontal axis of the volcano map is the fold-change (log2(B/A)) value showing the differential gene expression between different groups of samples. On the other hand, the vertical axis shows the statistically significant *p*-value representing the change in gene expression. The smaller the *p*-value, the -log10. The larger the (*p*-value), the more significant the difference. (**B**) Heat map for hierarchical clustering of differential gene expression. In the figure, each row represents a gene, and each column represents a sample. The color represents the expression level of the gene. Red represents a high expression level, while green represents a low expression level. On the left is the dendrogram of gene clustering. The closer the two gene branches are, the closer their expression levels are. A dendrogram for sample clustering is shown at the top, the name of the sample is shown at the bottom, and the two sample branches are separated from each other. The closer the branches, the closer the expression of the genes in the two samples. (**C**) Venn diagram was the intersection of the three gene sets: the plumbagin group compared with the control group, the cisplatin group compared with the control group and the cisplatin plus plumbagin group compared with the control group.

Plumbagin vs Control

Gene id	Gene Name	Fold Change	P Value	Change trend
ENSG00000207145	SNORA18	7379.466969	4.75E-05	up
ENSG00000000971	CFH	244.8078208	0.000215447	up
ENSG00000151491	EPS8	188.9146296	1.44E-05	up
ENSG00000095585	BLNK	168.6788817	1.98E-05	up
ENSG00000115414	FN1	48.94424235	0.000173305	up
ENSG00000261780	LINC02582	16.94160012	0.000127479	up
ENSG00000161798	AQP5	15.39040031	0.000642734	up
ENSG00000125144	MT1G	9.940785872	8.61E-07	up
ENSG00000166825	ANPEP	7.281591874	3.37E-07	up
ENSG00000124664	SPDEF	6.607865682	2.38E-08	up
ENSG00000146674	IGFBP3	0.243687294	1.12E-05	down
ENSG00000168675	LDLRAD4	0.238371142	1.91E-07	down
ENSG00000136048	DRAM1	0.234777588	0.000304495	down
ENSG00000108244	KRT23	0.232588117	2.47E-06	down
ENSG00000113269	RNF130	0.226766523	8.79E-05	down
ENSG00000266460	AC021506.1	0.202007501	0.000124644	down
ENSG00000260566	AC127459.1	0.18439872	8.97E-05	down
ENSG00000257529	RPL36A-HNRNPH2	0.110786092	9.27E-09	down
ENSG00000222328	RNU2-2P	0.048668264	0.000476609	down
ENSG00000269897	COMMD3-BMI1	1.71E-05	6.02E-11	down

Cisplatin vs Control

Gene id	Gene Name	Fold Change	P Value	Change trend
ENSG00000138685	FGF2	685.5109209	5.83E-21	up
ENSG00000101443	WFDC2	470.0203922	1.57E-08	up
ENSG00000134339	SAA2	301.1149516	1.77E-10	up
ENSG00000197249	SERPINA1	135.6399366	0.000166594	up
ENSG00000273333	AL662884.1	132.3190765	9.78E-05	up
ENSG00000173432	SAA1	74.116237	2.15E-10	up
ENSG00000124875	CXCL6	64.43397559	4.08E-06	up
ENSG00000156966	B3GNT7	62.20665353	2.66E-15	up
ENSG00000100985	MMP9	60.45628641	6.10E-08	up
ENSG00000184371	CSF1	45.97898304	0.002129846	up
ENSG00000105668	UPK1A	0.069166857	3.87E-11	down
ENSG00000161798	AQP5	0.065420618	5.99E-10	down
ENSG00000255730	AC011462.1	0.055432122	9.27E-11	down
ENSG00000248405	PRR5-ARHGAP8	0.052934352	0.001279518	down
ENSG00000167768	KRT1	0.043322866	2.08E-32	down
ENSG00000164687	FABP5	0.04162799	0.00000027	down
ENSG00000166634	SERPINB12	0.038757176	5.09E-14	down
ENSG00000273003	ARL2-SNX15	0.03832951	0.000115427	down
ENSG00000197953	AADACL2	0.019075406	0.000644157	down
ENSG00000257341	AL928654.3	0.00713142	0.000495141	down

Plumbagin+Cisplatin vs Control

Gene id	Gene Name	Fold Change	P Value	Change trend
ENSG00000173432	SAA1	9.686123316	6.46361E-06	up
ENSG00000100985	MMP9	7.667987499	1.18558E-10	up
ENSG00000184254	ALDH1A3	4.85542942	2.66128E-06	up
ENSG00000163739	CXCL1	4.738569961	5.69747E-08	up
ENSG00000271503	CCL5	4.678701211	2.45661E-09	up
ENSG00000120129	DUSP1	4.30628848	1.00522E-07	up
ENSG00000008517	IL32	4.158891446	4.37407E-07	up
ENSG00000185298	CCDC137	3.156660206	1.37568E-05	up
ENSG00000163430	FSTL1	3.13782788	3.78385E-05	up
ENSG00000166922	SC65	2.852372706	1.9708E-08	up
ENSG00000167377	ZNF23	0.346324905	4.10754E-06	down
ENSG00000143631	FLG	0.292333857	4.5114E-05	down
ENSG00000166634	SERPINB12	0.2835764	0.000120609	down
ENSG00000167768	KRT1	0.263943504	4.06575E-06	down
ENSG00000158985	CDC42SE2	0.219117865	1.50649E-13	down
ENSG00000277971	AC007731.4	0.141886192	2.07178E-05	down
ENSG00000273003	ARL2-SNX15	0.133968981	2.89202E-05	down
ENSG00000254788	CKLF-CMTM1	0.051217667	0.000154783	down
ENSG00000269897	COMMD3-BMI1	0.038286023	2.80764E-08	down
ENSG00000240963	AL645465.1	0.009028592	1.90834E-05	down

Figure 8. The top 10 upregulated mRNAs and top 10 downregulated mRNAs.

Biomarkers correlated with immune infiltration level

The associations between the expression of the mRNAs and the abundance of immune cells infiltration were analyzed using ssGSEA. As illustrated in the lollipop plot (Figure 13), the expression of AXL, SCG5, VOPP1, DCBLD2, DRAM1, DUSP1, AQP5 and BLNK exhibited a strong positive correlation with some immunocytes, including macrophages, cytotoxic cells, T cells, B cells, Th1 cells, Th2 cells, and NK cells (p-value < 0.05). These findings suggest that these mRNAs affect immune responses by influencing the infiltration of immunocytes into the microenvironment of oral squamous cell carcinoma.

DISCUSSION

Tongue squamous cell carcinoma is one of the most commonly diagnosed intraoral squamous cell carcinomas (25–40%). It is considered an aggressive form of squamous cell carcinoma with a five-year survival rate of less than 50% [31]. The tongue possesses a rich vascular, lymphatic network and a well-represented musculature. Therefore, tongue squamous cell carcinoma has an increased tendency for invasion and metastasis [32].

Compared to traditional preclinical experiments based on cell lines, the PDX models provide an important tool for tumor research, and the PDX models have emerged as pre-clinical models for cancer research. The PDX models maintain the heterogeneity and microenvironment of human tumors. Further, several studies have shown high consistency between pre-clinical experiments using PDX models and results of clinical treatment. Therefore, the PDX models are useful in studying tumor pathogenesis and developing personalized treatment [16, 17, 33]. The tumor model generated by transplanting tumor cell lines into mice is different from the primary tumor. Therefore, the drug dosage range tends to be different [33]. Therefore, the PDX model is a more reliable model for evaluating the anti-cancer effects of chemotherapeutic drugs [16, 17]. In addition, the PDX model plays a crucial role in investigating drug resistance in tumors [34].

Cisplatin is the most commonly used chemotherapy drug for TSCC. Moreover, it is used as the first-line agent for TSCC [35–37]. However, cisplatin is associated with toxic side effects, including peripheral neuropathy (CIPN), nephrotoxicity, ototoxicity, cardio-toxicity, and intestinal damage [38–41]. Moreover, with the passage of medication time and the increase of drug dose, drug resistance greatly limits the effectiveness of chemotherapy [42]. Oral squamous cell carcinoma shows an initial response rate to cisplatin of 80.6% [43]. However, more than 70% of the patients eventually relapse due to acquired drug resistance [44, 45]. Therefore, it is urgent to study a new treatment strategy to overcome the chemoresistance of TSCC and reduce the toxicity and side effects of cisplatin.

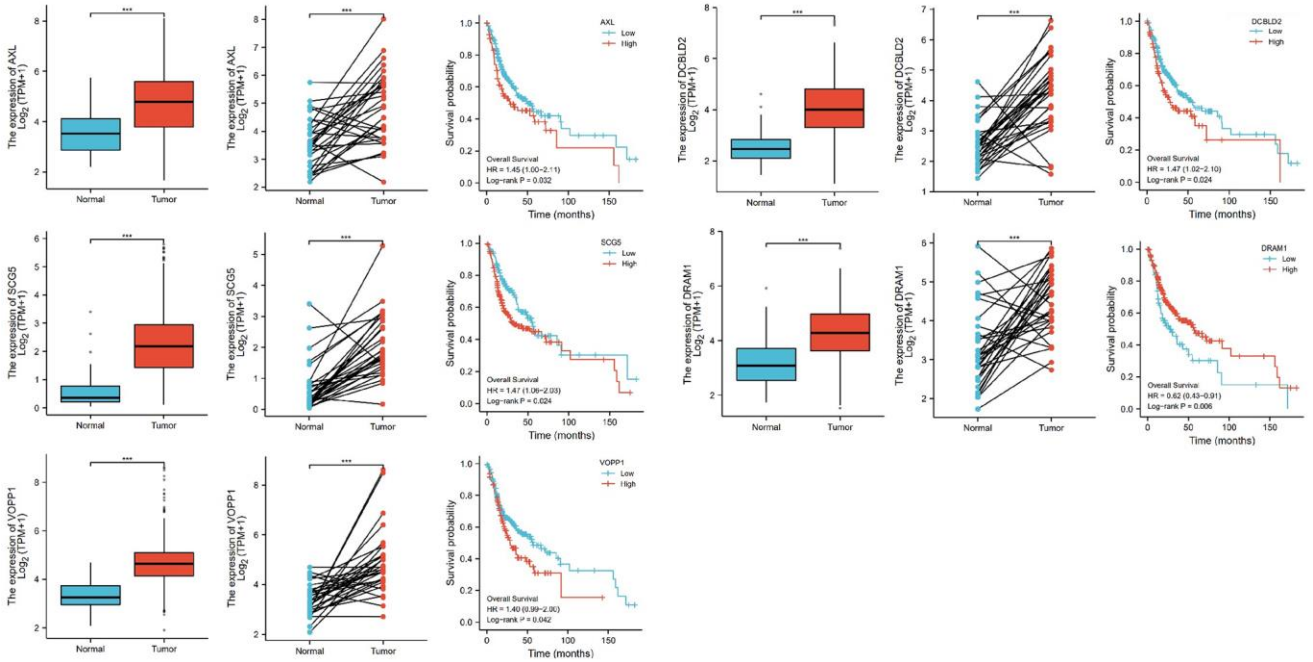

Figure 9. The relative expression levels of 5 genes (AXL, SCG5, VOPP1, DCBLD2, DRAM1) in cancer tissues and normal tissues, and their influence on survival probability. ***P < 0.00.

Plumbagin is a small molecular weight compound derived from the roots of Plumbago zeylanica L, a traditional Chinese medicine (TCM). Plumbagin has been reported to have anti-cancer effects in various cancer types [22]. Plumbagin played anticancer activity via many molecular mechanisms, such as apoptosis, autophagy pathway, antiangiogenesis pathway, anti-invasion [46]. Our previous study demonstrated that plumbagin induced apoptosis and autophagy by generating reactive oxygen species in TSCC cells, and inhibiting the AKT/mTOR signaling pathway. Further, plumbagin showed synergistic effects with cisplatin in inhibiting the growth of TSCC cells [27]. In this study, we continued to study the anticancer efficacy of plumbagin on the TSCC models.

To the best of our knowledge, this is the first study exploring the synergistic effects of cisplatin and

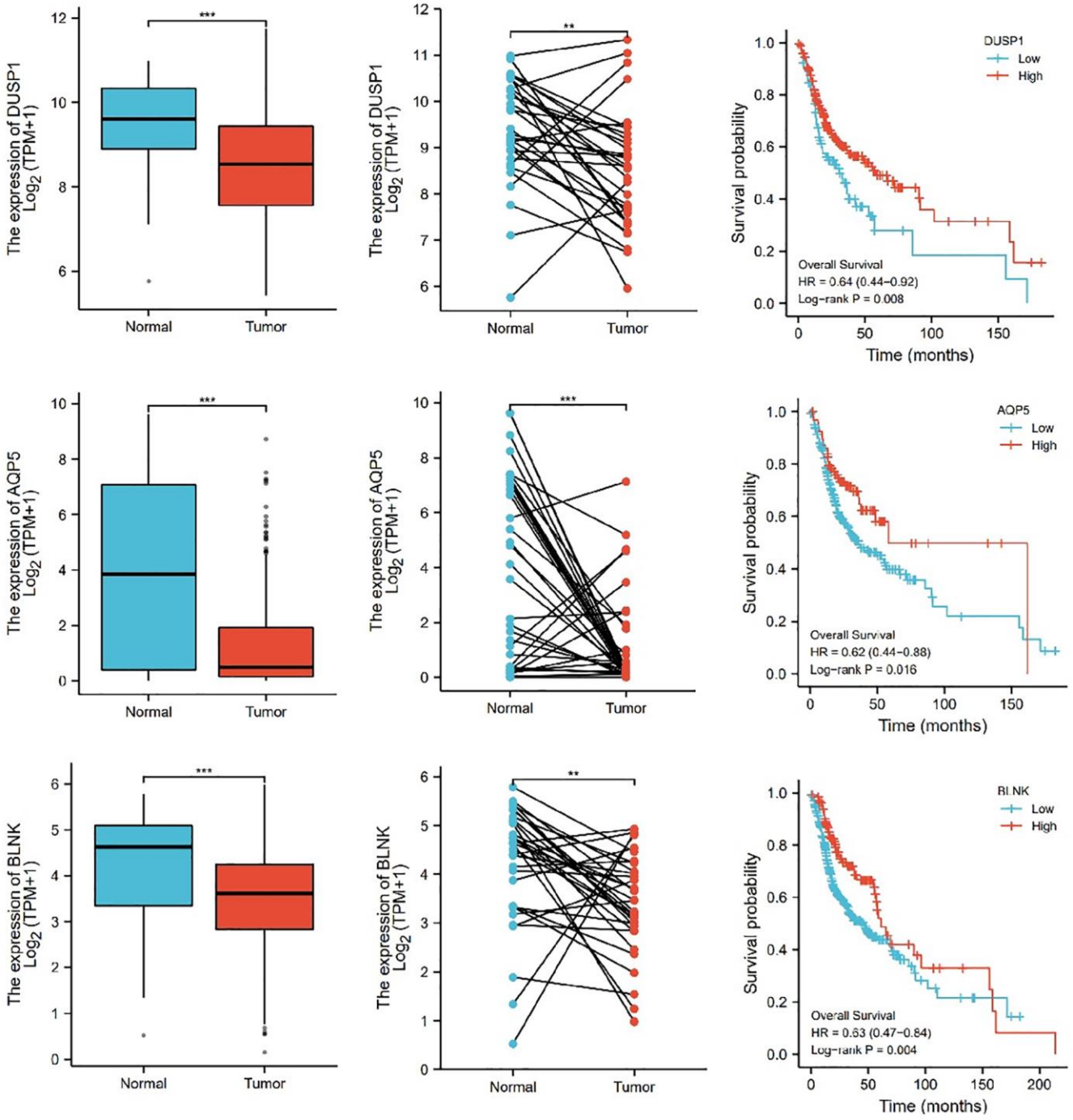

Figure 10. The relative expression levels of 3 (DUSP1, AQP5, BLNK) genes in cancer tissues and normal tissues, and their influence on survival probability. $^{***}P < 0.001$.

plumbagin in TSCC-PDX models. The results demonstrated an inhibitory effect on tumor growth in plumbagin treatment group. However, the plumbagin plus cisplatin group showed synergistic effects with the greatest inhibitory effects on tumor growth. The body weight in the treatment groups remained unchanged compared to the control group. Furthermore, the H&E staining of the heart, liver, spleen, lungs, and kidneys in the four groups did not show any organ-related toxicity. Taken together, these results demonstrated that plumbagin has anti-tumor effects on TSCC PDX models. In addition, plumbagin enhances the anti-tumor

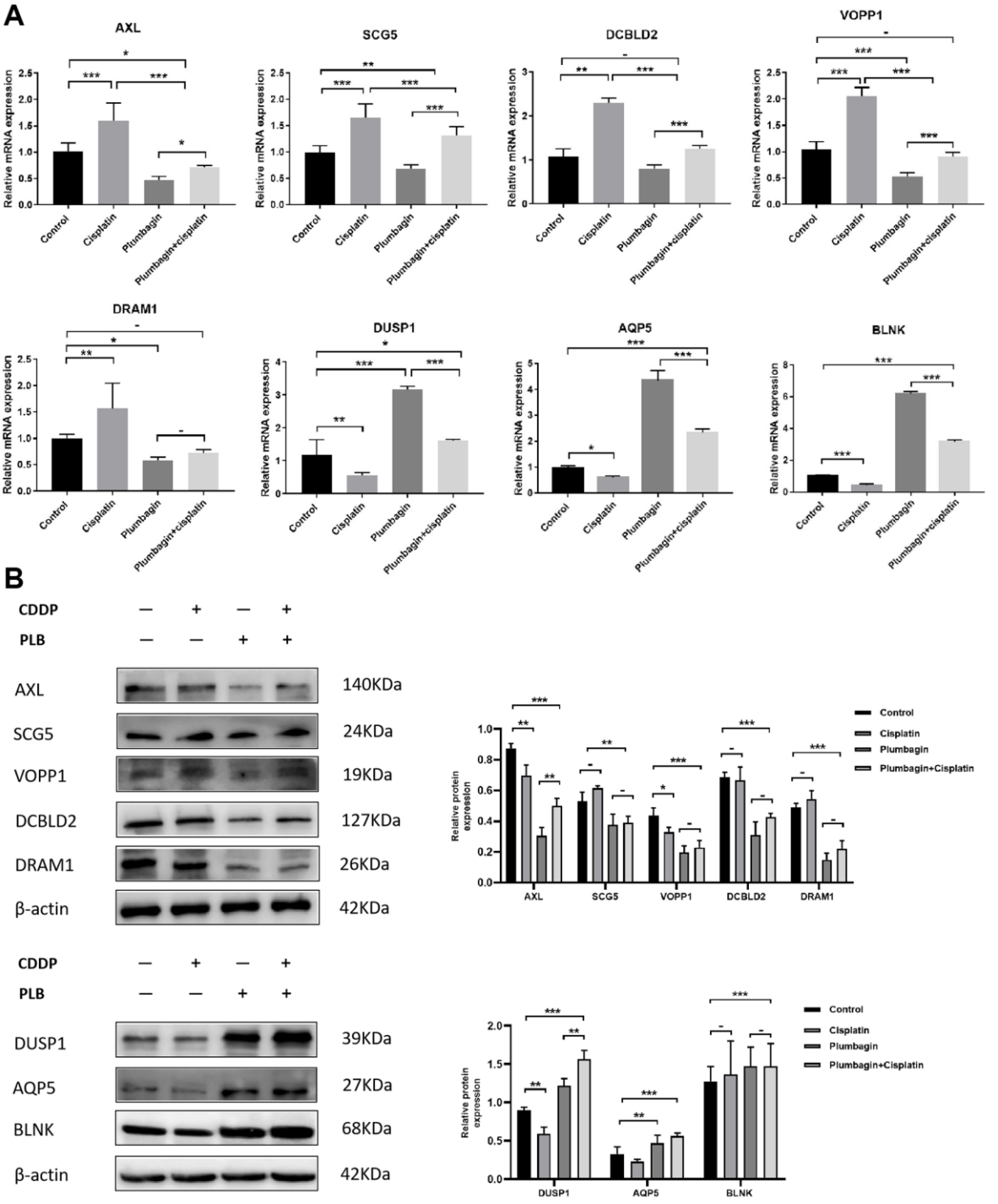

Figure 11. Relative expression of AXL, SCG5, VOPP1, DCBLD2, DRAM1, DUSP1, AQP5, BLNK in the four treatment groups. Treatment groups referred to PDX tumors harvested from mice. (**A**) The expression of differential genes in four groups of PDX models by RT-qPCR. (**B**) The expression of differential genes in four groups of PDX models by Western blotting. The quantitative data are shown as the mean ± SD of 3 independent experiments. $^{***}P < 0.001$; $^{**}P < 0.01$; $^{*}P < 0.05$; –, no statistical difference.

effects of cisplatin and is not associated with severe toxicity. Ki67 is a related antigen of proliferating cells, which is mainly used to mark cells in the proliferation cycle. The higher the positive rate of Ki67, the faster the tumor growth, the poorer the tissue differentiation ability, and the higher the degree of malignancy [47]. The immunohistochemistry results revealed that plumbagin could effectively inhibit the proliferation of tumor cells in the TSCC PDX model. Furthermore, plumbagin combined with cisplatin could enhance the

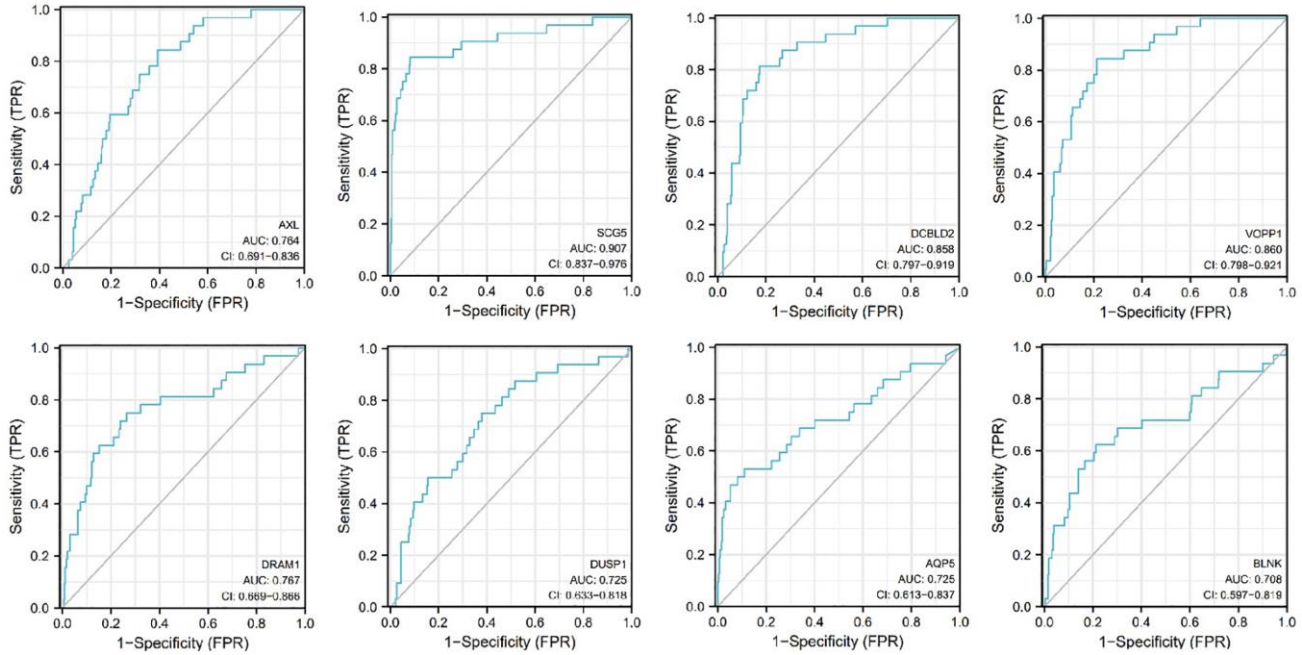

Figure 12. Receiver operating characteristic curves (ROC) for the AXL, SCG5, VOPP1, DCBLD2, DRAM1, DUSP1, AQP5, BLNK in the patients with oral squamous cell carcinoma.

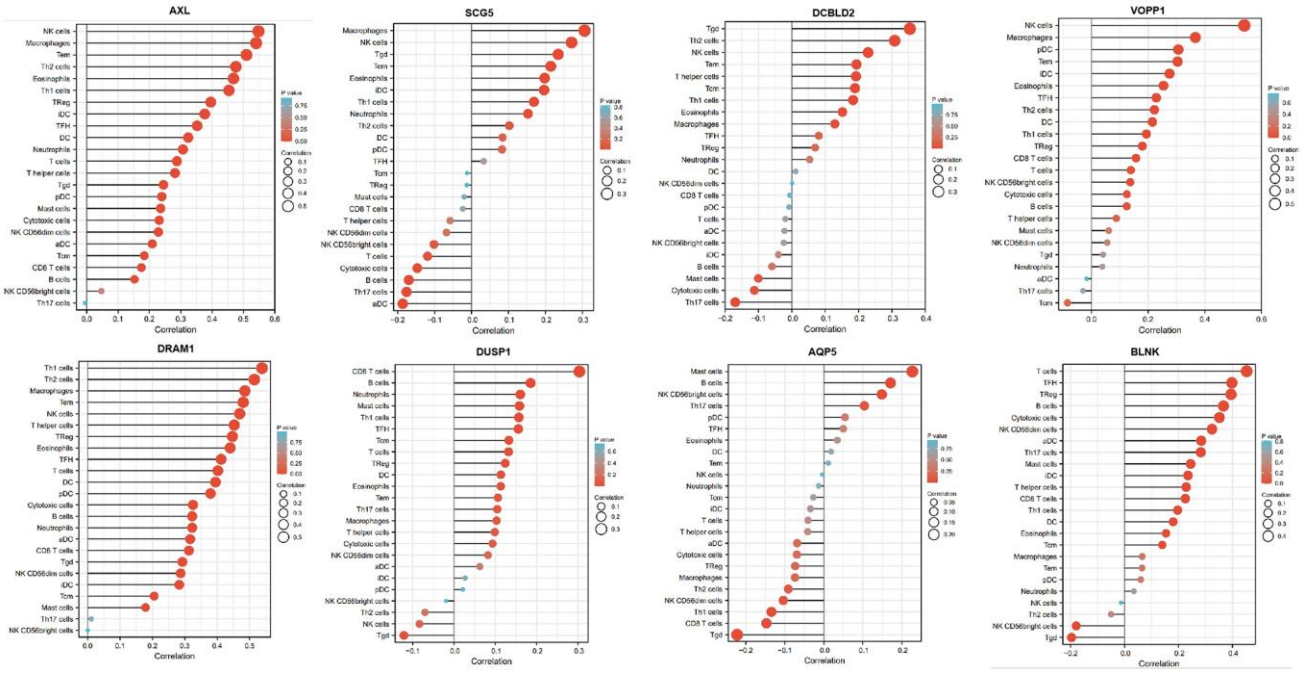

Figure 13. Relationship between 8 mRNAs and immune infiltration. The lollipop plot shows the correlation between AXL, SCG5, VOPP1, DCBLD2, DRAM1, DUSP1, AQP5 and BLNK expression and 24 immune cell subsets infiltration. The size of dots indicates the absolute Spearman *r* value.

anti-proliferative effects of cisplatin. And we found that plumbagin could inhibit Akt/mTOR pathway in TSCC PDX models. Moreover, plumbagin showed synergistic effects with cisplatin in inhibiting Akt/mTOR pathway of TSCC PDX models. Therefore, this study is of great significance to the clinical application of plumbagin.

Next-generation sequencing (NGS) is a technology that allows thousands to billions of DNA fragments to be sequenced simultaneously. Next-generation sequencing is also known as high-throughput or massively parallel sequencing [48]. At present, several studies combine the PDX model with NGS to research disease diagnosis and treatment [49]. In this study, NGS was used to study the anticancer efficacy of plumbagin and the additive effects of plumbagin and cisplatin in TSCC-PDX models. In this study, we used NGS and bioinformatics approaches to analyze and compare the expression of mRNA in tumor tissues between the cisplatin, plumbagin and their combination treatment group with the control group. Overall, 124 upregulated mRNAs and 59 downregulated mRNAs were identified in the plumbagin group compared with the control group. In addition, 383 upregulated mRNAs and 364 downregulated mRNAs were identified in the cisplatin group compared with the control group. Furthermore, 17 upregulated mRNAs and 23 downregulated mRNAs were identified in the cisplatin plus plumbagin group compared with the control group. Eight genes were shown to be related to the prognosis in patients with tongue squamous cell carcinoma (AXL, SCG5, VOPP1, DCBLD2, DRAM, DUSP1, AQP5, BLNK).

Anexelekto (AXL) is a member of the Tyro3, AXL, and Mertk family of receptor tyrosine kinases (RTKs). It is associated with tumor cell growth, migration, invasion, and immune suppression [47, 50–52]. In addition, several studies reveal that secretogranin V (SCG5) is related to tumor prognosis [53, 54]. Moreover, Prosurvival Protein 1 (VOPP1) shows increased expression in various cancer types, such as squamous cell carcinoma, colorectal cancer, glioblastoma and gastric cancer [55]. VOPP1 enhances cell proliferation, migration and inhibits apoptosis [56, 57]. In addition, DCBLD2 is a neuropilin-related transmembrane protein expressed in endothelial cells (ECs). The DCBLD2 gene is involved in angiogenesis, tumorigenesis, tumor progression, and could be exploited as a therapeutic target for the regulation of angiogenesis [58, 59]. Moreover, DNA damage-regulated autophagy modulator 1 (DRAM1) plays an important role in autophagy and tumor progression [60]. Previous studies report that DRAM is a direct target of p53 and a critical factor for p53-dependent apoptosis and autophagy [61, 62]. The expression of AXL, SCG5, VOPP1, DCBLD2 and DRAM in oral squamous cell carcinoma were significantly higher in the TCGA database than in normal tissues. Moreover, these genes were related to the prognosis of patients. Furthermore, the RT-qPCR analysis and WB analysis revealed that cisplatin did not inhibit the expression of these genes. However, treatment using both plumbagin and cisplatin inhibited the expression of these genes.

Mitogen-activated protein kinase (MAPK) is essential for immune cell function. The activity of MAPK is controlled by dual-specificity phosphatases (DUSPs) [63]. Among them, DUSP1 has been shown to be related to cell proliferation, differentiation, transformation, stress response, inflammation, cycle arrest, and apoptosis [64, 65]. In addition, aquaporin 5 (AQP5), a member of the aquaporin family, is a cell membrane protein involved in the transport of water molecules [66]. Previous studies reported that AQP5 was associated with the formation and progression of various cancers [67, 68]. B-cell linker protein (BLNK) is an adaptor protein and it plays a crucial role in the B cell antigen receptor signaling pathway [69]. In fact, BLNK is considered an initiator of critical tumor suppressors. In addition, a previous study reported that BLNK could induce apoptosis [70]. The expression of DUSP1, AQP5, and BLNK in malignant tumors of the oral region was significantly lower than in normal tissues, according to the TCGA database. Furthermore, these genes were related to the prognosis of patients. The RT-qPCR analysis and WB analysis revealed that cisplatin did not promote the expression of these genes. However, a combination of plumbagin and cisplatin promoted the expression of these genes.

We used the ROC curve to detect the accuracy of the above 8 mRNAs in the diagnosis of oral squamous cell carcinoma. The areas under the ROC curve of AXL, SCG5, DCBLD2, VOPP1, DRAM1, DUSP1, AQP5, and BLNK in the detection of oral squamous cell carcinoma were 0.764, 0.907, 0.858, 0.860, 0.767, 0.725, 0.725 and 0.708, respectively. The area values under the ROC curve of the 8 mRNAs are all greater than 0.7. Therefore, these mRNAs were promising biomarkers in the screening and diagnosis of TSCC.

The mortality of patients with advanced or recurrent TSCC could increase drastically to 92% [71]. The introduction of immunotherapy (IT) recently provided a further treatment option for advanced and recurrent solid cancers, including TSCC [72]. Recent studies also mention the tumor microenvironment as a potential source for identifying new biomarkers [73]. Therefore, we analyzed the associations between the expression of the above mRNA and the infiltration of immune cells. We found the expression of these mRNA exhibited a strong positive correlation with some immunocytes,

including macrophages, cytotoxic cells, T cells, B cells, Th1 cells, Th2 cells, and NK cells. Therefore, these mRNAs were shown to affect immune responses by influencing the infiltration of immunocytes into the microenvironment of oral squamous cell carcinoma. This study provides potential targets that could be exploited in future research to determine how plumbagin could be used as an immunotherapeutic agent in tongue squamous cell carcinoma, though the specific inhibitory mechanism needs to be further explored.

CONCLUSION

In this study, 14 TSCC PDX models were successfully generated. Furthermore, plumbagin could inhibit the growth of TSCC PDX models and inhibited Akt/mTOR pathway. Moreover, plumbagin showed synergistic effects with cisplatin in inhibiting the growth of the PDX model of TSCC. Finally, the NGS demonstrated that plumbagin could enhance the effects of cisplatin by affecting genes such as AXL, SCG5, VOPP1, DCBLD2, DRAM1, DUSP1, AQP5, and BLNK which are related to the diagnosis, growth, prognosis, and immune cell infiltration of TSCC. Therefore, this study is of great significance to the clinical application of plumbagin.

Abbreviations

HNSCC: Head and neck squamous cell carcinoma; TSCC: Tongue squamous cell carcinoma; PDX: Patient-derived xenograft; NGS: Next-generation sequencing; TCM: Traditional Chinese medicine; HE: Hematoxylin-Eosin; IHC: Immunohistochemistry; PCR: Polymerase Chain Reaction; RT-qPCR: Reverse Transcription-Quantitative Polymerase Chain Reaction; ROC: Receiver operating characteristic; AUC: Area under the curve; AXL: Anexelekto; RTKs: Receptor tyrosine kinases; SCG5: Secretogranin V; VOPP1: Prosurvival Protein 1; ECs: Endothelial cells; DRAM1: DNA damage-regulated autophagy modulator 1; MAPK: Mitogen-activated protein kinase; DUSPs: Dual-specificity phosphatases; AQP5: Aquaporin 5; BLNK: B-cell linker protein.

AUTHOR CONTRIBUTIONS

YX and JQ conceived and designed the experiments. YX, and QJ performed most of the experiments and data analysis. CL collected the clinical samples and information. JQ provided administrative support. All authors wrote and reviewed this manuscript.

CONFLICTS OF INTEREST

The authors declare no conflicts of interest related to this study.

ETHICAL STATEMENT AND CONSENT

Written informed consent was obtained from all participants or their legal guardians prior to sample collection. All experimental protocols were approved by the Ethics Committee of First Affiliated Hospital of Nanchang University (2022) CDYFYYLK (11-002) and conducted in accordance with the principles of the World Medical Association Declaration of Helsinki. Animal experiments were approved by the Medical Ethics Committee of First Affiliated Hospital of Nanchang University (CDYFY-IACUC-202211QR016) that was conducted according to the ARRIVE guidelines. And all methods were carried out in accordance with relevant guidelines and regulations.

FUNDING

The present study was supported by the National Natural Science Foundation of China (Grant No. 82260194), Jiangxi Provincial Key R&D Plan (Grant No. 20212BBG71005), Jiangxi Provincial Science and Technology Department Science and Technology Innovation Base Construction Project (No. 20221ZDG020068) and the Special Fund for Postgraduate Innovation in Jiangxi Province (Grant No. YC2019-S103).

REFERENCES

1. Siegel RL, Miller KD, Jemal A. Cancer statistics, 2018. CA Cancer J Clin. 2018; 68:7–30. https://doi.org/10.3322/caac.21442 PMID:29313949

2. Du L, Liang Q, Ge S, Yang C, Yang P. The growth inhibitory effect of human gingiva-derived mesenchymal stromal cells expressing interferon-β on tongue squamous cell carcinoma cells and xenograft model. Stem Cell Res Ther. 2019; 10:224. https://doi.org/10.1186/s13287-019-1320-z PMID:31358054

3. Cancer Genome Atlas Network. Comprehensive genomic characterization of head and neck squamous cell carcinomas. Nature. 2015; 517:576–82. https://doi.org/10.1038/nature14129 PMID:25631445

4. Li X, Rui B, Cao Y, Gong X, Li H. Long non-coding RNA LINC00152 acts as a sponge of miRNA-193b-3p to promote tongue squamous cell carcinoma progression. Oncol Lett. 2020; 19:2035–42. https://doi.org/10.3892/ol.2020.11293 PMID:32194700

5. Omori H, Nishio M, Masuda M, Miyachi Y, Ueda F, Nakano T, Sato K, Mimori K, Taguchi K, Hikasa H,

Nishina H, Tashiro H, Kiyono T, et al. YAP1 is a potent driver of the onset and progression of oral squamous cell carcinoma. Sci Adv. 2020; 6:eaay3324. https://doi.org/10.1126/sciadv.aay3324 PMID:32206709

6. Ye X, Wang X, Lu R, Zhang J, Chen X, Zhou G. CD47 as a potential prognostic marker for oral leukoplakia and oral squamous cell carcinoma. Oncol Lett. 2018; 15:9075–80. https://doi.org/10.3892/ol.2018.8520 PMID:29805639

7. Jeon JH, Kim MG, Park JY, Lee JH, Kim MJ, Myoung H, Choi SW. Analysis of the outcome of young age tongue squamous cell carcinoma. Maxillofac Plast Reconstr Surg. 2017; 39:41. https://doi.org/10.1186/s40902-017-0139-8 PMID:29302590

8. Fu X, Chen S, Chen W, Yang Z, Song M, Li H, Zhang H, Yao F, Su X, Liu T, Yang AK. Clinical analysis of second primary gingival squamous cell carcinoma after radiotherapy. Oral Oncol. 2018; 84:20–4. https://doi.org/10.1016/j.oraloncology.2018.06.018 PMID:30115471

9. Lu Z, Yan W, Liang J, Yu M, Liu J, Hao J, Wan Q, Liu J, Luo C, Chen Y. Nomogram Based on Systemic Immune-Inflammation Index to Predict Survival of Tongue Cancer Patients Who Underwent Cervical Dissection. Front Oncol. 2020; 10:341. https://doi.org/10.3389/fonc.2020.00341 PMID:32219070

10. Warnakulasuriya S. Living with oral cancer: epidemiology with particular reference to prevalence and life-style changes that influence survival. Oral Oncol. 2010; 46:407–10. https://doi.org/10.1016/j.oraloncology.2010.02.015 PMID:20403722

11. Bachar G, Hod R, Goldstein DP, Irish JC, Gullane PJ, Brown D, Gilbert RW, Hadar T, Feinmesser R, Shpitzer T. Outcome of oral tongue squamous cell carcinoma in patients with and without known risk factors. Oral Oncol. 2011; 47:45–50. https://doi.org/10.1016/j.oraloncology.2010.11.003 PMID:21167767

12. Vered M, Dayan D, Dobriyan A, Yahalom R, Shalmon B, Barshack I, Bedrin L, Talmi YP, Taicher S. Oral tongue squamous cell carcinoma: recurrent disease is associated with histopathologic risk score and young age. J Cancer Res Clin Oncol. 2010; 136:1039–48. https://doi.org/10.1007/s00432-009-0749-3 PMID:20054559

13. Lilja-Fischer JK, Ulhøi BP, Alsner J, Stougaard M, Thomsen MS, Busk M, Lassen P, Steiniche T, Nielsen VE, Overgaard J. Characterization and radiosensitivity of HPV-related oropharyngeal squamous cell carcinoma patient-derived xenografts. Acta Oncol. 2019; 58:1489–94. https://doi.org/10.1080/0284186X.2019.1660802 PMID:31510843

14. Fan J, Lee HO, Lee S, Ryu DE, Lee S, Xue C, Kim SJ, Kim K, Barkas N, Park PJ, Park WY, Kharchenko PV. Linking transcriptional and genetic tumor heterogeneity through allele analysis of single-cell RNA-seq data. Genome Res. 2018; 28:1217–27. https://doi.org/10.1101/gr.228080.117 PMID:29898899

15. Yuan Y. Spatial Heterogeneity in the Tumor Microenvironment. Cold Spring Harb Perspect Med. 2016; 6:a026583. https://doi.org/10.1101/cshperspect.a026583 PMID:27481837

16. Hidalgo M, Amant F, Biankin AV, Budinská E, Byrne AT, Caldas C, Clarke RB, de Jong S, Jonkers J, Mælandsmo GM, Roman-Roman S, Seoane J, Trusolino L, Villanueva A. Patient-derived xenograft models: an emerging platform for translational cancer research. Cancer Discov. 2014; 4:998–1013. https://doi.org/10.1158/2159-8290.CD-14-0001 PMID:25185190

17. Burgenske DM, Monsma DJ, MacKeigan JP. Patient-Derived Xenograft Models of Colorectal Cancer: Procedures for Engraftment and Propagation. Methods Mol Biol. 2018; 1765:307–14. https://doi.org/10.1007/978-1-4939-7765-9_20 PMID:29589317

18. Izumchenko E, Paz K, Ciznadija D, Sloma I, Katz A, Vasquez-Dunddel D, Ben-Zvi I, Stebbing J, McGuire W, Harris W, Maki R, Gaya A, Bedi A, et al. Patient-derived xenografts effectively capture responses to oncology therapy in a heterogeneous cohort of patients with solid tumors. Ann Oncol. 2017; 28:2595–605. https://doi.org/10.1093/annonc/mdx416 PMID:28945830

19. Sun CY, Zhang QY, Zheng GJ, Feng B. Phytochemicals: Current strategy to sensitize cancer cells to cisplatin. Biomed Pharmacother. 2019; 110:518–27. https://doi.org/10.1016/j.biopha.2018.12.010 PMID:30530287

20. AlQathama A, Ezuruike UF, Mazzari ALD, Yonbawi A, Chieli E, Prieto JM. Effects of Selected Nigerian Medicinal Plants on the Viability, Mobility, and Multidrug-Resistant Mechanisms in Liver, Colon, and Skin Cancer Cell Lines. Front Pharmacol. 2020; 11:546439. https://doi.org/10.3389/fphar.2020.546439 PMID:33071779

21. Cheng YT, Yang CC, Shyur LF. Phytomedicine-Modulating oxidative stress and the tumor microenvironment for cancer therapy. Pharmacol Res. 2016; 114:128–43. https://doi.org/10.1016/j.phrs.2016.10.022 PMID:27794498

22. Wang T, Qiao H, Zhai Z, Zhang J, Tu J, Zheng X, Qian N, Zhou H, Lu E, Tang T. Plumbagin Ameliorates Collagen-Induced Arthritis by Regulating Treg/Th17 Cell Imbalances and Suppressing Osteoclastogenesis. Front Immunol. 2019; 9:3102. https://doi.org/10.3389/fimmu.2018.03102 PMID:30671063

23. Cao YY, Yu J, Liu TT, Yang KX, Yang LY, Chen Q, Shi F, Hao JJ, Cai Y, Wang MR, Lu WH, Zhang Y. Plumbagin inhibits the proliferation and survival of esophageal cancer cells by blocking STAT3-PLK1-AKT signaling. Cell Death Dis. 2018; 9:17. https://doi.org/10.1038/s41419-017-0068-6 PMID:29339720

24. Hafeez BB, Zhong W, Mustafa A, Fischer JW, Witkowsky O, Verma AK. Plumbagin inhibits prostate cancer development in TRAMP mice via targeting PKCε, Stat3 and neuroendocrine markers. Carcinogenesis. 2012; 33:2586–92. https://doi.org/10.1093/carcin/bgs291 PMID:22976928

25. Pan ST, Qin Y, Zhou ZW, He ZX, Zhang X, Yang T, Yang YX, Wang D, Zhou SF, Qiu JX. Plumbagin suppresses epithelial to mesenchymal transition and stemness via inhibiting Nrf2-mediated signaling pathway in human tongue squamous cell carcinoma cells. Drug Des Devel Ther. 2015; 9:5511–51. https://doi.org/10.2147/DDDT.S89621 PMID:26491260

26. Pan ST, Qin Y, Zhou ZW, He ZX, Zhang X, Yang T, Yang YX, Wang D, Qiu JX, Zhou SF. Plumbagin induces G2/M arrest, apoptosis, and autophagy via p38 MAPK- and PI3K/Akt/mTOR-mediated pathways in human tongue squamous cell carcinoma cells. Drug Des Devel Ther. 2015; 9:1601–26. https://doi.org/10.2147/DDDT.S76057 PMID:25834400

27. Xue D, Pan ST, Zhou X, Ye F, Zhou Q, Shi F, He F, Yu H, Qiu J. Plumbagin Enhances the Anticancer Efficacy of Cisplatin by Increasing Intracellular ROS in Human Tongue Squamous Cell Carcinoma. Oxid Med Cell Longev. 2020; 2020:5649174. https://doi.org/10.1155/2020/5649174 PMID:32308804

28. Xin Y, Li S, Jiang Q, Hu F, He Y, Zhang J. Establishment of a Jaw Fibrosarcoma Patient-Derived Xenograft and Evaluation of the Tumor Suppression Efficacy of Plumbagin Against Jaw Fibrosarcoma. Front Oncol. 2020; 10:1479. https://doi.org/10.3389/fonc.2020.01479 PMID:32974176

29. Ferreira NH, Furtado RA, Ribeiro AB, de Oliveira PF, Ozelin SD, de Souza LDR, Neto FR, Miura BA, Magalhães GM, Nassar EJ, Tavares DC. Europium(III)-doped yttrium vanadate nanoparticles reduce the toxicity of cisplatin. J Inorg Biochem. 2018; 182:9–17. https://doi.org/10.1016/j.jinorgbio.2018.01.014 PMID:29407869

30. Jiang ZB, Xu C, Wang W, Zhang YZ, Huang JM, Xie YJ, Wang QQ, Fan XX, Yao XJ, Xie C, Wang XR, Yan PY, Ma YP, et al. Plumbagin suppresses non-small cell lung cancer progression through downregulating ARF1 and by elevating $CD8^+$ T cells. Pharmacol Res. 2021; 169:105656. https://doi.org/10.1016/j.phrs.2021.105656 PMID:33964470

31. Ion Ciucă Mărăşescu FI, Marasescu PC, Matei M, Florescu AM, Margaritescu C, Petrescu SMS, Dumitrescu CI. Epidemiological and Histopathological Aspects of Tongue Squamous Cell Carcinomas-Retrospective Study. Curr Health Sci J. 2018; 44:211–24. https://doi.org/10.12865/CHSJ.44.03.03 PMID:30647940

32. Lim MS. Re: Correlational of oral tongue cancer inversion with matrix metalloproteinases (MMPs) and vascular endothelial growth factor (VEGF) expression, by Kim S-H, Cho NH, Kim K, et al. J Surg Oncol. 2006; 93:253–4. https://doi.org/10.1002/jso.20462 PMID:16496361

33. Yin Z, Maswikiti EP, Liu Q, Bai Y, Li X, Qi W, Liu L, Ma Y, Chen H. Current research developments of patient-derived tumour xenograft models (Review). Exp Ther Med. 2021; 22:1206. https://doi.org/10.3892/etm.2021.10640 PMID:34584551

34. Bertotti A, Migliardi G, Galimi F, Sassi F, Torti D, Isella C, Corà D, Di Nicolantonio F, Buscarino M, Petti C, Ribero D, Russolillo N, Muratore A, et al. A molecularly annotated platform of patient-derived xenografts ("xenopatients") identifies HER2 as an effective therapeutic target in cetuximab-resistant colorectal cancer. Cancer Discov. 2011; 1:508–23. https://doi.org/10.1158/2159-8290.CD-11-0109 PMID:22586653

35. Yu M, Xiao L, Chen Y, Wang H, Gao Y, Wang A. Identification of a potential target for treatment of squamous cell carcinoma of the tongue: follistatin. Br J Oral Maxillofac Surg. 2020; 58:437–42.

https://doi.org/10.1016/j.bjoms.2020.01.028
PMID:32115303

36. Gibson MK, Li Y, Murphy B, Hussain MH, DeConti RC, Ensley J, Forastiere AA, and Eastern Cooperative Oncology Group. Randomized phase III evaluation of cisplatin plus fluorouracil versus cisplatin plus paclitaxel in advanced head and neck cancer (E1395): an intergroup trial of the Eastern Cooperative Oncology Group. J Clin Oncol. 2005; 23:3562–7. https://doi.org/10.1200/JCO.2005.01.057 PMID:15908667

37. Jacobs C, Lyman G, Velez-García E, Sridhar KS, Knight W, Hochster H, Goodnough LT, Mortimer JE, Einhorn LH, Schacter L. A phase III randomized study comparing cisplatin and fluorouracil as single agents and in combination for advanced squamous cell carcinoma of the head and neck. J Clin Oncol. 1992; 10:257–63. https://doi.org/10.1200/JCO.1992.10.2.257 PMID:1732427

38. Sałat K. Chemotherapy-induced peripheral neuropathy-part 2: focus on the prevention of oxaliplatin-induced neurotoxicity. Pharmacol Rep. 2020; 72:508–27. https://doi.org/10.1007/s43440-020-00106-1 PMID:32347537

39. Zhang JJ, Wang JQ, Xu XY, Yang JY, Wang Z, Jiang S, Wang YP, Zhang J, Zhang R, Li W. Red ginseng protects against cisplatin-induced intestinal toxicity by inhibiting apoptosis and autophagy via the PI3K/AKT and MAPK signaling pathways. Food Funct. 2020; 11:4236–48. https://doi.org/10.1039/d0fo00469c PMID:32355945

40. Shaker ME, Shaaban AA, El-Shafey MM, El-Mesery ME. The selective c-Met inhibitor capmatinib offsets cisplatin-nephrotoxicity and doxorubicin-cardiotoxicity and improves their anticancer efficacies. Toxicol Appl Pharmacol. 2020; 398:115018. https://doi.org/10.1016/j.taap.2020.115018 PMID:32333917

41. Mondal J, Khuda-Bukhsh AR. Cisplatin and farnesol co-encapsulated PLGA nano-particles demonstrate enhanced anti-cancer potential against hepatocellular carcinoma cells in vitro. Mol Biol Rep. 2020; 47:3615–28. https://doi.org/10.1007/s11033-020-05455-x PMID:32314187

42. Florea AM, Büsselberg D. Cisplatin as an anti-tumor drug: cellular mechanisms of activity, drug resistance and induced side effects. Cancers (Basel). 2011; 3:1351–71. https://doi.org/10.3390/cancers3011351 PMID:24212665

43. Zhong LP, Zhang CP, Ren GX, Guo W, William WN Jr, Sun J, Zhu HG, Tu WY, Li J, Cai YL, Wang LZ, Fan XD, Wang ZH, et al. Randomized phase III trial of induction chemotherapy with docetaxel, cisplatin, and fluorouracil followed by surgery versus up-front surgery in locally advanced resectable oral squamous cell carcinoma. J Clin Oncol. 2013; 31:744–51. https://doi.org/10.1200/JCO.2012.43.8820 PMID:23129742

44. Abdelmaksoud NM, Abulsoud AI, Doghish AS, Abdelghany TM. From resistance to resilience: Uncovering chemotherapeutic resistance mechanisms; insights from established models. Biochim Biophys Acta Rev Cancer. 2023. [Epub ahead of print]. https://doi.org/10.1016/j.bbcan.2023.188993 PMID:37813202

45. Fan S, Liu B, Sun L, Lv XB, Lin Z, Chen W, Chen W, Tang Q, Wang Y, Su Y, Jin S, Zhang D, Zhong J, et al. Mitochondrial fission determines cisplatin sensitivity in tongue squamous cell carcinoma through the BRCA1-miR-593-5p-MFF axis. Oncotarget. 2015; 6:14885–904. https://doi.org/10.18632/oncotarget.3659 PMID:25912308

46. Yin Z, Zhang J, Chen L, Guo Q, Yang B, Zhang W, Kang W. Anticancer Effects and Mechanisms of Action of Plumbagin: Review of Research Advances. Biomed Res Int. 2020; 2020:6940953. https://doi.org/10.1155/2020/6940953 PMID:33344645

47. Li H, Ren G, Cai R, Chen J, Wu X, Zhao J. A correlation research of Ki67 index, CT features, and risk stratification in gastrointestinal stromal tumor. Cancer Med. 2018; 7:4467–74. https://doi.org/10.1002/cam4.1737 PMID:30123969

48. Gu W, Miller S, Chiu CY. Clinical Metagenomic Next-Generation Sequencing for Pathogen Detection. Annu Rev Pathol. 2019; 14:319–38. https://doi.org/10.1146/annurev-pathmechdis-012418-012751 PMID:30355154

49. Khandelwal G, Girotti MR, Smowton C, Taylor S, Wirth C, Dynowski M, Frese KK, Brady G, Dive C, Marais R, Miller C. Next-Generation Sequencing Analysis and Algorithms for PDX and CDX Models. Mol Cancer Res. 2017; 15:1012–6. https://doi.org/10.1158/1541-7786.MCR-16-0431 PMID:28442585

50. Colavito SA. AXL as a Target in Breast Cancer Therapy. J Oncol. 2020; 2020:5291952.

https://doi.org/10.1155/2020/5291952
PMID:32148495

51. Myers SH, Brunton VG, Unciti-Broceta A. AXL Inhibitors in Cancer: A Medicinal Chemistry Perspective. J Med Chem. 2016; 59:3593–608. https://doi.org/10.1021/acs.jmedchem.5b01273 PMID:26555154

52. Chang H, An R, Li X, Lang X, Feng J, Lv M. Anti-Axl monoclonal antibodies attenuate the migration of MDA-MB-231 breast cancer cells. Oncol Lett. 2021; 22:749. https://doi.org/10.3892/ol.2021.13010 PMID:34539853

53. Yang W, Zhou W, Zhao X, Wang X, Duan L, Li Y, Niu L, Chen J, Zhang Y, Han Y, Fan D, Hong L. Prognostic biomarkers and therapeutic targets in oral squamous cell carcinoma: a study based on cross-database analysis. Hereditas. 2021; 158:15. https://doi.org/10.1186/s41065-021-00181-1 PMID:33892811

54. Xu JS, Liao KL, Wang X, He J, Wang XZ. Combining bioinformatics techniques to explore the molecular mechanisms involved in pancreatic cancer metastasis and prognosis. J Cell Mol Med. 2020; 24:14128–38. https://doi.org/10.1111/jcmm.16023 PMID:33164330

55. Hu P, Wang B, Chen T, Xu Y, Zheng G, Zhu Y, Du X. RNA polymerase II subunit 3 regulates vesicular, overexpressed in cancer, prosurvival protein 1 expression to promote hepatocellular carcinoma. J Int Med Res. 2021; 49:300060521990512. https://doi.org/10.1177/0300060521990512 PMID:33845647

56. Xu J, Chen Z, Fang Z, Chen S, Guo Y, Liu X, Chen K, Chen S. Long non-coding RNA OIP5-AS1 promotes the progression of esophageal cancer by regulating miR-30a/VOPP1 expression. Oncol Lett. 2021; 22:651. https://doi.org/10.3892/ol.2021.12912 PMID:34386073

57. Gao C, Pang M, Zhou Z, Long S, Dong D, Yang J, Cao M, Zhang C, Han S, Li L. Epidermal growth factor receptor-coamplified and overexpressed protein (VOPP1) is a putative oncogene in gastric cancer. Clin Exp Med. 2015; 15:469–75. https://doi.org/10.1007/s10238-014-0320-7 PMID:25398664

58. Dong Y, Ma WM, Shi ZD, Zhang ZG, Zhou JH, Li Y, Zhang SQ, Pang K, Li BB, Zhang WD, Fan T, Zhu GY, Xue L, et al. Role of NRP1 in Bladder Cancer Pathogenesis and Progression. Front Oncol. 2021; 11:685980. https://doi.org/10.3389/fonc.2021.685980 PMID:34249735

59. Xie P, Yuan FQ, Huang MS, Zhang W, Zhou HH, Li X, Liu ZQ. DCBLD2 Affects the Development of Colorectal Cancer via EMT and Angiogenesis and Modulates 5-FU Drug Resistance. Front Cell Dev Biol. 2021; 9:669285. https://doi.org/10.3389/fcell.2021.669285 PMID:34095137

60. Geng J, Zhang R, Yuan X, Xu H, Zhu Z, Wang X, Wang Y, Xu G, Guo W, Wu J, Qin ZH. DRAM1 plays a tumor suppressor role in NSCLC cells by promoting lysosomal degradation of EGFR. Cell Death Dis. 2020; 11:768. https://doi.org/10.1038/s41419-020-02979-9 PMID:32943616

61. Wang Y, Yao Y, Li R, Wu B, Lu H, Cheng J, Liu Z, Du J. Different effects of anti-VEGF drugs (Ranibizumab, Aflibercept, Conbercept) on autophagy and its effect on neovascularization in RF/6A cells. Microvasc Res. 2021; 138:104207. https://doi.org/10.1016/j.mvr.2021.104207 PMID:34119535

62. Lee HY, Oh SH. Autophagy-mediated cytoplasmic accumulation of p53 leads to apoptosis through DRAM-BAX in cadmium-exposed human proximal tubular cells. Biochem Biophys Res Commun. 2021; 534:128–33. https://doi.org/10.1016/j.bbrc.2020.12.019 PMID:33321290

63. Goel S, Saheb Sharif-Askari F, Saheb Sharif Askari N, Madkhana B, Alwaa AM, Mahboub B, Zakeri AM, Ratemi E, Hamoudi R, Hamid Q, Halwani R. SARS-CoV-2 Switches 'on' MAPK and NFκB Signaling via the Reduction of Nuclear DUSP1 and DUSP5 Expression. Front Pharmacol. 2021; 12:631879. https://doi.org/10.3389/fphar.2021.631879 PMID:33995033

64. Theodosiou A, Ashworth A. MAP kinase phosphatases. Genome Biol. 2002; 3:REVIEWS3009. https://doi.org/10.1186/gb-2002-3-7-reviews3009 PMID:12184814

65. Saxena M, Mustelin T. Extracellular signals and scores of phosphatases: all roads lead to MAP kinase. Semin Immunol. 2000; 12:387–96. https://doi.org/10.1006/smim.2000.0219 PMID:10995585

66. Direito I, Madeira A, Brito MA, Soveral G. Aquaporin-5: from structure to function and dysfunction in cancer. Cell Mol Life Sci. 2016; 73:1623–40. https://doi.org/10.1007/s00018-016-2142-0 PMID:26837927

67. Jensen HH, Login FH, Koffman JS, Kwon TH, Nejsum LN. The role of aquaporin-5 in cancer cell migration: A potential active participant. Int J Biochem Cell Biol. 2016; 79:271–6.

https://doi.org/10.1016/j.biocel.2016.09.005
PMID:27609140

68. Li N, Xu X, Yang H, Wang H, Ouyang Y, Zhou Y, Peng C, Yuan Z, He C, Zeng C, Hong J. Activation of Aquaporin 5 by carcinogenic Helicobacter pylori infection promotes epithelial-mesenchymal transition via the MEK/ERK pathway. Helicobacter. 2021; 26:e12842. https://doi.org/10.1111/hel.12842 PMID:34331360

69. Thomsen EA, Rovsing AB, Anderson MV, Due H, Huang J, Luo Y, Dybkaer K, Mikkelsen JG. Identification of BLNK and BTK as mediators of rituximab-induced programmed cell death by CRISPR screens in GCB-subtype diffuse large B-cell lymphoma. Mol Oncol. 2020; 14:1978–97. https://doi.org/10.1002/1878-0261.12753 PMID:32585766

70. Übelhart R, Werner M, Jumaa H. Assembly and Function of the Precursor B-Cell Receptor. Curr Top Microbiol Immunol. 2016; 393:3–25. https://doi.org/10.1007/82_2015_475 PMID:26415650

71. Weckx A, Riekert M, Grandoch A, Schick V, Zöller JE, Kreppel M. Time to recurrence and patient survival in recurrent oral squamous cell carcinoma. Oral Oncol. 2019; 94:8–13. https://doi.org/10.1016/j.oraloncology.2019.05.002 PMID:31178216

72. Ferris RL. Immunology and Immunotherapy of Head and Neck Cancer. J Clin Oncol. 2015; 33:3293–304. https://doi.org/10.1200/JCO.2015.61.1509 PMID:26351330

73. Gavrielatou N, Doumas S, Economopoulou P, Foukas PG, Psyrri A. Biomarkers for immunotherapy response in head and neck cancer. Cancer Treat Rev. 2020; 84:101977. https://doi.org/10.1016/j.ctrv.2020.101977 PMID:32018128

SUPPLEMENTARY MATERIALS

Supplementary Figures

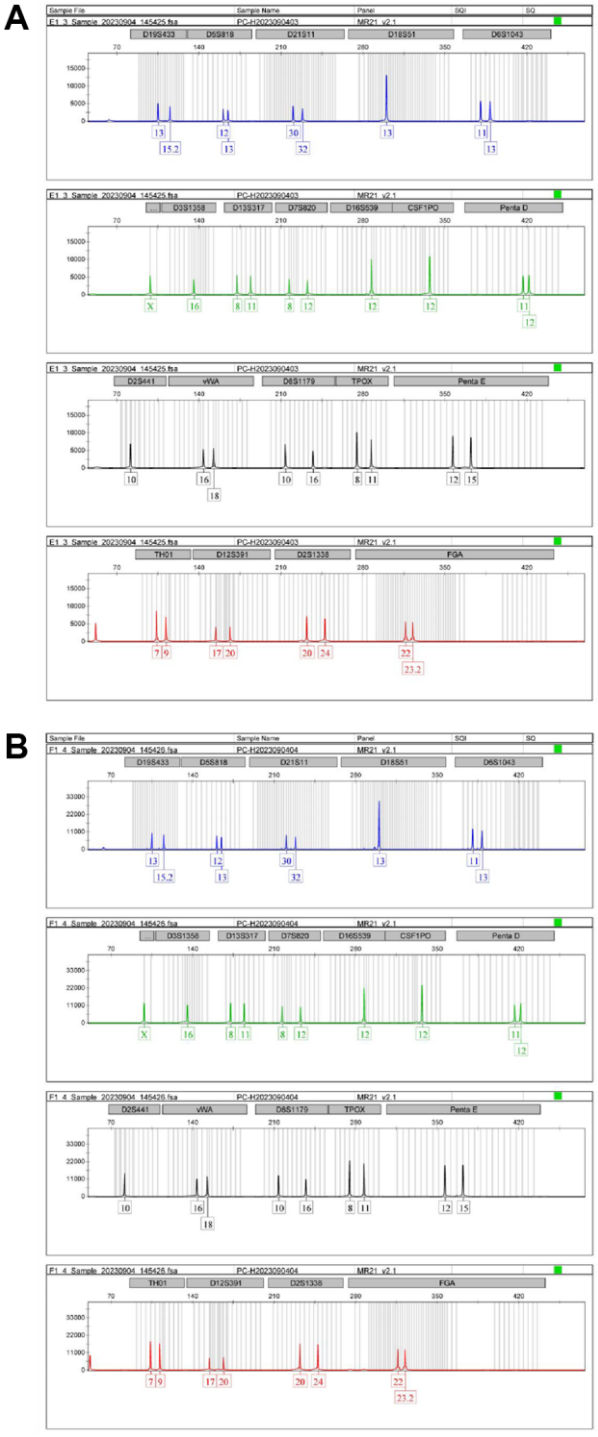

Supplementary Figure 1. PDX tissue and tumor tissue are the same individual origin by STR profile. (**A**) Short tandem repeat (STR) profile of patient tissue. (**B**) Short tandem repeat (STR) profile of PDX model.

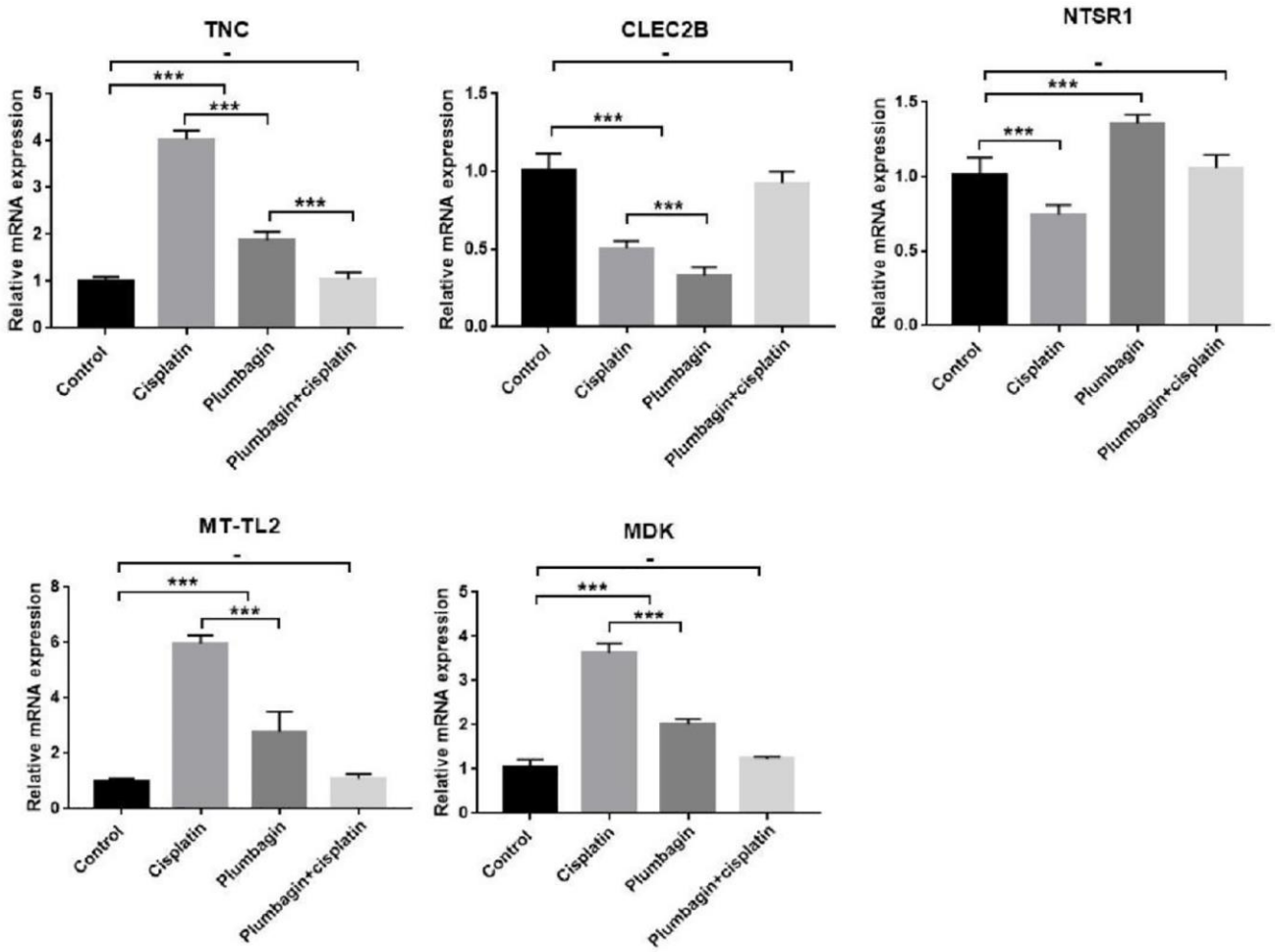

Supplementary Figure 2. Relative expression of TNC, CLEC2B, NTSR1, MT-TL2 and MDK in the four treatment groups by RT-qPCR. Treatment groups referred to PDX tumors harvested from mice. ***$P < 0.00$; −, no statistical difference.

Supplementary Tables

Please browse Full Text version to see the data of Supplementary Tables 1 and 2.

Supplementary Table 1. Expression of the differential genes in the plumbagin group compared with the control group.

Supplementary Table 2. Expression of the differential genes in the cisplatin group compared with the control group.

Supplementary Table 3. Expression of the differential genes in the plumbagin+cisplatin group compared with the control group.

Gene ID	Gene name	Fold change	log2 (Fold change)	*P* Value	Change trend
ENSG00000173432	SAA1	9.686123316	3.27591937	6.46E-06	up
ENSG00000100985	MMP9	7.667987499	2.938847985	1.19E-10	up
ENSG00000184254	ALDH1A3	4.85542942	2.279598895	2.66E-06	up
ENSG00000163739	CXCL1	4.738569961	2.244451738	5.70E-08	up
ENSG00000271503	CCL5	4.678701211	2.226108099	2.46E-09	up
ENSG00000120129	DUSP1	4.30628848	2.10644497	1.01E-07	up
ENSG00000008517	IL32	4.158891446	2.056199029	4.37E-07	up
ENSG00000185298	CCDC137	3.156660206	1.658398972	1.38E-05	up
ENSG00000163430	FSTL1	3.13782788	1.649766218	3.78E-05	up
ENSG00000166922	SCG5	2.852372706	1.512162504	1.9708E-08	up
ENSG00000161798	AQP5	2.804080912	1.487527979	2.2671E-07	up
ENSG00000095585	BLNK	2.766098807	1.467852692	5.45E-05	up
ENSG00000103034	NDRG4	2.752057809	1.460510775	0.00015106	up
ENSG00000255529	POLR2M	2.524976652	1.336270047	4.33E-17	up
ENSG00000167565	SERTAD3	2.119449764	1.083689772	2.48E-05	up
ENSG00000244462	RBM12	2.107639548	1.075628156	9.72E-07	up
ENSG00000006118	TMEM132A	2.017572951	1.012620839	4.40E-07	up
ENSG00000114439	BBX	0.496389635	−1.010455103	1.41E-05	down
ENSG00000114857	NKTR	0.472072373	−1.08292004	7.12E-07	down
ENSG00000073282	TP63	0.448430565	−1.15704348	0.00019702	down
ENSG00000163349	HIPK1	0.438690444	−1.188724815	2.91E-05	down
ENSG00000119938	PPP1R3C	0.428411092	−1.222932262	1.74E-09	down
ENSG00000175003	SLC22A1	0.407248439	−1.296018926	1.60E-06	down
ENSG00000170525	PFKFB3	0.39475456	−1.340972165	4.70E-05	down
ENSG00000147789	ZNF7	0.377585301	−1.40512549	1.46E-08	down
ENSG00000155508	CNOT8	0.370807387	−1.431258108	1.28E-13	down
ENSG00000118520	ARG1	0.360160124	−1.473289635	7.08E-11	down
ENSG00000134765	DSC1	0.352667077	−1.503621194	4.94E-05	down
ENSG00000127129	EDN2	0.350755349	−1.511462988	0.0001282	down
ENSG00000167601	AXL	0.346349511	−1.52969946	4.55E-09	down
ENSG00000167377	ZNF23	0.346324905	−1.529801958	4.11E-06	down

ENSG00000143631	FLG	0.292333857	−1.77431117	4.51E-05	down
ENSG00000166634	SERPINB12	0.2835764	−1.818190621	0.00012061	down
ENSG00000167768	KRT1	0.263943504	−1.921698934	4.07E-06	down
ENSG00000158985	CDC42SE2	0.219117865	−2.190220982	1.51E-13	down
ENSG00000277971	AC007731.4	0.141886192	−2.817193895	2.07E-05	down
ENSG00000273003	ARL2-SNX15	0.133968981	−2.900029096	2.89E-05	down
ENSG00000254788	CKLF-CMTM1	0.051217667	−4.287214651	0.00015478	down
ENSG00000269897	COMMD3-BMI1	0.038286023	−4.707038383	2.81E-08	down
ENSG00000240963	AL645465.1	0.009028592	−6.791283228	1.91E-05	down